Rapid coastal erosion of ice-bonded deposits on Pelly Island, southeastern Beaufort Sea, Inuvialuit Settlement Region, western Canadian Arctic

By
François Malenfant

A Thesis Submitted to
Saint Mary's University, Halifax, Nova Scotia
in Partial Fulfillment of the Requirements for
the Degree of Master of Science in Applied Science

April, 2022 Halifax, Nova Scotia

Approved: Dr. Danika van Proosdij
Supervisor
Department of Geography
And Environmental Sciences

Approved: Dustin Whalen
Supervisory Committee Member
Geological Survey of Canada

Approved: Dr. Gavin Manson
Supervisory Committee Member
Geological Survey of Canada

Approved: Dr. Jason Rhinelander
Supervisory Committee Member
Division of Engineering

Approved: Dr. Don Forbes
External Examiner
Geological Survey of Canada

Date: April, 2022

Abstract

Extensive erosion of lacustrine coastlines on Pelly Island (NWT, Canada)

By Francois Malenfant

This paper quantifies rates of shoreline change and investigates the influence of surficial geology on shoreline dynamics between 1950 and 2018 on Pelly Island, located 10 km off the Mackenzie Delta. Long-term changes in shoreline position were calculated using imagery analysis and *Analysing Moving Boundaries Using R* (AMBUR), and short-term volumetric erosion was calculated using UAV-SfM methods. The influence of shoreline exposure to predominant storm direction and influence of surficial geology were examined for Northwest and Southeast zones. The average annual linear regression rate (LRR) rate during the 1950-2018 observation period was -3.8 $m \cdot a^{-1}$. The end point rate (EPR) was calculated for six observation periods: 1950-1972, 1972-1985, 1985-2000, 2000-2018, 2013-2018. A mean EPR of -5.5 ± 0.7 $m \cdot a^{-1}$ was calculated for the 2000-2018 period, and a maximum retreat rate of 46.7 ± 2.1 $m \cdot a^{-1}$ was recorded during the 2013-2018 observation period.

April, 2022

Acknowledgements:

I would like to thank my partner Jess, my brother Julien, my friends, my parents and grandparents for their ongoing support and encouragement during my thesis. I thank my thesis supervisor Danika for being a patient, adaptable, and empathetic instructor, and for her willingness to impart her world-class geoscience knowledge with me. I also thank my co-supervisors Dustin Whalen and Gavin Manson for their support and guidance. I am grateful for the opportunity to have partaken in Saint Mary's Master of Applied Sciences Coop Program, which allowed me to partake in a three-month Arctic expedition to the Northwest Territories and Yukon coast. During this time, I worked alongside professional geoscientists from around the globe, and was very fortunate to work with indigenous communities of the Inuvialuit Settlement Region. I would like to thank the contributions of the following institutions: Arora Research Institute; Tuktoyaktuk Hunters and Trappers Committee; community support from the Inuvialuit Settlement Region, Natural Resources Canada (NRCan) Climate Change Geoscience Program, The Polar Continental Shelf Program (PCSP), Natural Environment Research Council (NERC), Indian and Northern Affairs Canada (INAC), Fisheries and Oceans Canada (DFO), Parks Canada (PC). I thank Vladimir Kostylev (NRCan), Sam Gruben, Weronika Murray for their help conducting field work, and I thank Paul Fraser (NRCan) Greg Baker (Saint Mary's University) and Graeme Matheson (Saint Mary's University) for their technical support. The research is carried out under the NWT Science Licence 16286.

Contents

Chapter 1: Introduction

During the 1950-2000 period permafrost coastlines along the Circum-Arctic were eroding at a mean rate of -0.5 $m \cdot a^{-1}$ (Lantuit et al. 2012). The highest rates of coastal erosion in the circum-Arctic during the 1950 to 2000 period were observed in the Canadian Beaufort Sea (-1.1 $m \cdot a^{-1}$) (Lantuit et al. 2012). Research in Canada has mostly focused on Arctic coastal sites where retreat rates have been previously documented, such as the Beaufort Sea coast (e.g., Lim et al., 2020; Solomon, 2005; Manson and Solomon, 2007; Forbes et al., 1995; Couture et al. 2018; Lantuit and Pollard, 2008; Irrgang et al. 2018; Tanski et al. 2019). The Quaternary geology of the Beaufort Sea region was initially investigated by the Geological Survey of Canada in the 1960s due to active oil and gas exploration. Exploration throughout the region emphasized the importance of surficial geology studies to effectively manage transportation. This led to the compilation of observations of stratigraphic sequences of Quaternary deposits and landforms; the distribution of permafrost and ground ice in relation to Quaternary deposits; and the effects of modern geomorphological processes on the landscape (Rampton, 1988). Our research focuses on Pelly Island (Figure 1.1), the largest of three islands located in the outer island zone of the Mackenzie Delta Estuary in the Canadian Arctic. Previous research found that the outer islands of the Mackenzie Delta had a mean rate of retreat of 1.5 $m \cdot a^{-1}$ during the 1972 to 2000 period, and Pelly Island had the highest maximum retreat rate reported for the entire Beaufort-Mackenzie shoreline in the 1972-2000 period (22.5 $m \cdot a^{-1}$) (Solomon, 2005). Pelly Island has been identified as being ecologically and biologically significant in the Beaufort Sea and is the only outer Island of the Mackenzie Delta to lie within the boundaries of the Okeevik sub-area of the Tarium Niryutait Marine Protected Area (Integrated Ocean Management Plan for the Beaufort Sea 2003) (Figure 1.1).

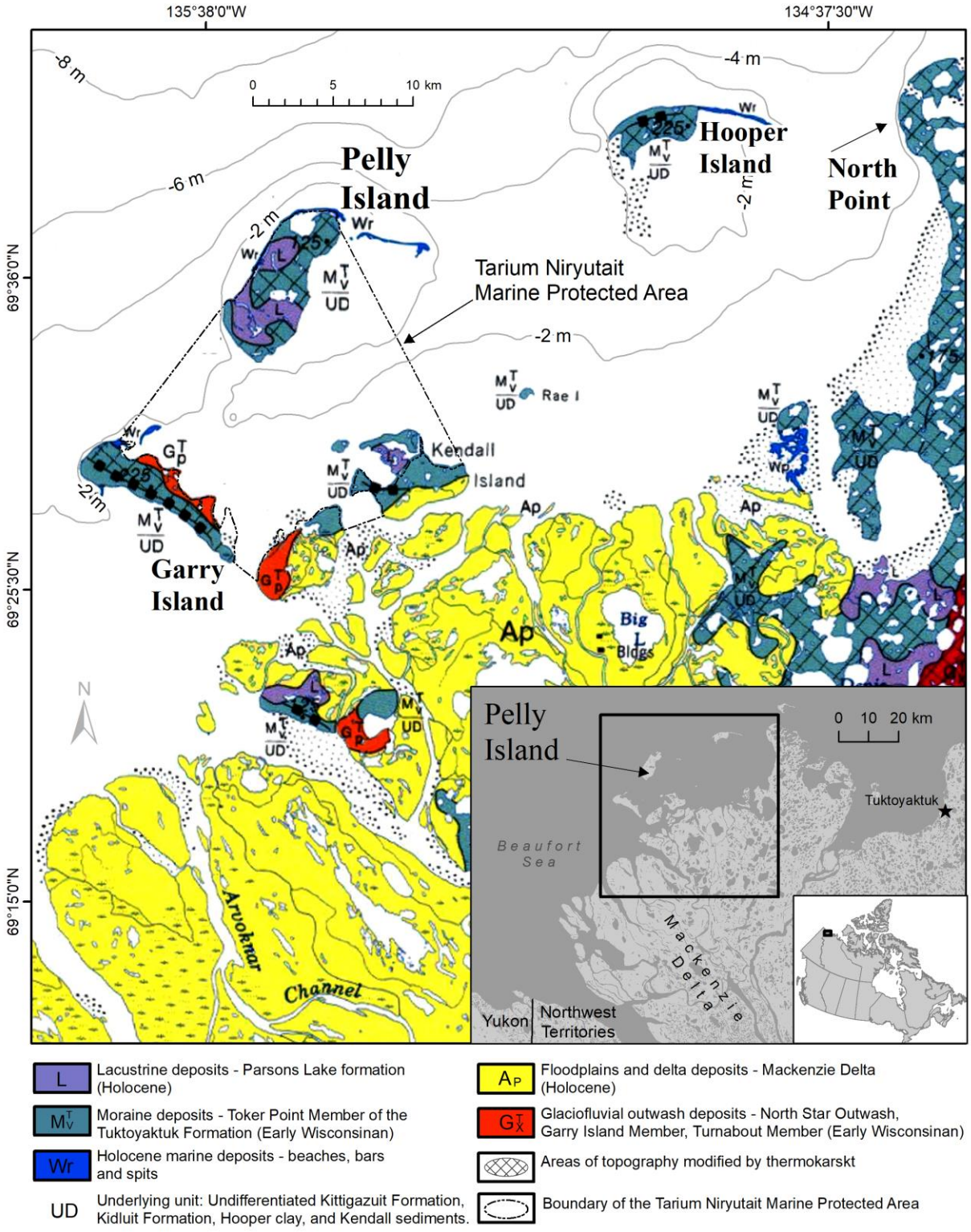

Figure 1.1: Pelly Island surficial geology map modified from 1950 Geological Survey of Canada map 1647A (Rampton 1987). Pelly Island is located 10 km from the Mackenzie Delta front and lies within the boundaries of the Tarium Niryutait Marine Protected Area (GEBCO 2m isobath).

1.1 Approaches to the study of Arctic Coastal Dynamics

Prior to 1950, the Davisian Cycle of erosion was the primary framework applied to the study of coastal geomorphology and viewed landscapes as being primarily influenced by orderly stages of uplift, planation and sea level change (Davidson-Arnott 2010). It interpreted coastlines as a simple system which moved toward a more static equilibrium by straightening coastlines through the action of waves and currents, which worked to erode headlands and build bay- mouth barriers. This framework for landform studies has mostly been replaced by the paradigm of denudation chronology, which involves the detailed reconstruction of coastal landscape evolution using concepts of erosion based on landforms rather than stratigraphy. The combination of the paradigm of denudation chronology and the advent of new technology in remote sensing, coring, and sediment dating has allowed for the detailed description of glacial history and post-glacial evolution of coasts worldwide (Davidson-Arnott 2010). Arctic coasts have been studied for over two centuries, with the first academic studies framing the basic knowledge of Arctic coasts by Adams (1807), Leffingwell (1919) and Hmiznikov (1937). Knowledge of Arctic coastal dynamics was then broadened by authors such as Mackay (1963, 1986), Are (1988) and Rampton (1988).

1.2 Arctic coastal environment and systems

In the past two decades there has been an acceleration of erosion of ice-rich permafrost in the Arctic due to changing environmental factors such as declining sea ice, warming temperatures and increased forcing events (Lantuit et al. 2012, Khon et al. 2014, Johannssen et al. 2002, Manson et al. 2005). Arctic permafrost is receiving greater attention because its degradation both onshore and offshore can release greenhouse gases, which contribute to a warming climate (Rachold et al,

2005). Detailed investigations of the Earth's climate show that we are currently experiencing a warming period due to increasing quantities of greenhouse gases (Overland et al., 2011). This trend is amplified in the Arctic because of a positive feedback system (Figure 1.2). Increasing air temperatures result in the decrease of land and sea ice cover, leading to a decrease in reflective surfaces and an increase in absorption of solar radiation, which in turn increases air temperatures.

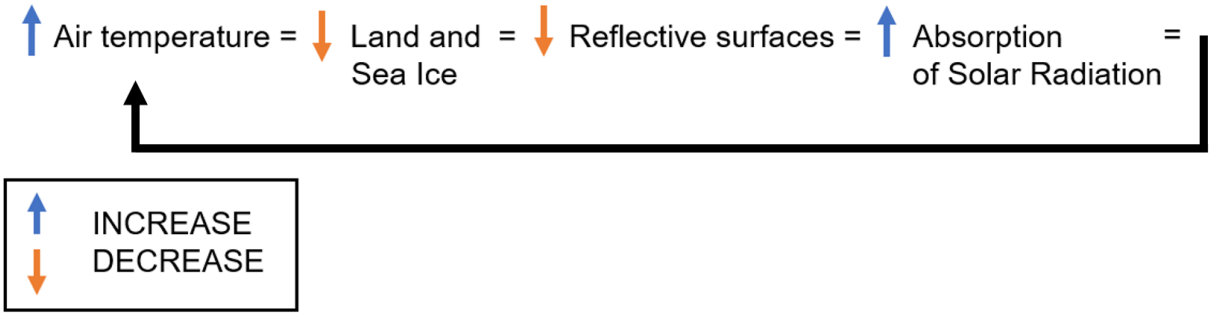

Figure 1.2: The positive feedback system observed in the Arctic due to a warming climate.

The evidence for the impact of a warming climate in the Arctic environment over the past four decades is found in the decreasing sea ice extent, increasing soil temperature, increasing air temperature, and increasing precipitation patterns (Konopczak et. al., 2014). Polar regions are considered to have a strong influence on global climate because of this negative feedback system (Overland et al., 2011). Changes in global and regional climate will impact the physical processes, biodiversity and socio-economic development in Arctic coastal zones (Rachold et al. 2005).

1.3 Environmental forcing and coastal processes in the Arctic

The coastal zone is the area where energy exchanges between land and ocean occur, and in the Arctic (like in many other places in the world) it is the location with the most human activity (Rachold et al. 2005). However, the Arctic coastal zone differs from temperate regions due to the

presence of ice in marine and terrestrial environments (sea ice, permafrost and ground ice) and the short open water season (3-4 months). Therefore, an understanding of environmental forcing and coastal processes specific to the Arctic is important for managing Arctic coastal hazards and human impacts on the coastal zone.

Continental shelves and margins are the interface between land and the open ocean, an area which is important for sequestering sediments, recycling and sequestering organic carbon, biological productivity, and human activity (Berner 1982; Lavoie et al., 2010). The Arctic has the largest proportion (30%) of continental shelf for all the world oceans and represents 20% of the worlds continental shelf area (Macdonald et al., 1998). This thesis focuses on the Canadian portion of the Beaufort Shelf, also known as the Mackenzie Shelf, which is the largest shelf on the North American side of the Arctic Ocean. The Mackenzie Shelf has been extensively studied and has multiple sediment sources, dynamic transport processes, and an open communication with the Arctic Ocean. It is estimated that about half of the terrestrial sediment supply is trapped in the Mackenzie Delta with about 40% deposited to the shelf and the remainder brought to the shelf edge (Macdonald et al., 1998).

International Arctic Coastal projects are compiling data from numerous coastal monitoring sites across the Arctic, with the goal of estimating sediment and carbon fluxes on a Circum-Arctic scale (Reimnitz et al. 1998; Rachold 2000; MacDonald et al. 1998, Brown et al. 2003; Jorgenson et al. 2003). The erosion of permafrost rich coasts (highest rates observed in Beaufort and Laptev Seas) is assumed to play a major role in the material budget of the Arctic Ocean (Rachold et al., 2005). Studies have shown that coastal erosion is an important component of sediment and total organic carbon to Arctic Seas (Brown et al. 2003; Grigoriev and Rachold 2003; Jorgenson et al. 2003; Rachold et al. 2003). Arctic permafrost is thought to store approximately half of global soil

organic carbon, and its degradation both onshore and offshore can release greenhouse gases (Rachold et al, 2005). Degradation of exposed subaerial and subaqueous permafrost has been found to increase while in contact with relatively warmer and saline seawater (Rachold et al, 2005), making permafrost degradation in the coastal zone of significance. Degradation of permafrost can transfer soil carbon to the ocean, where it is either buried in nearshore shelf sediments, exported offshore or mineralized by bacteria then released to the atmosphere as a greenhouse gas furthering the current warming climate (Tanski et al., 2019).

Changes in Arctic climate can trigger many environmental responses. Arctic coastlines are highly variable both temporally and spatially (Rachold et al. 2000; Solomon 2005; Lantuit & Pollard 2008; Harper et al. 1985; Solomon and Covill 1995; Solomon et al. 1994). Spatial variability is mainly due to variations in lithology, geocryology (ground ice, sea ice and permafrost), and geomorphology, shoreline planform (shoreline orientation and exposure) all of which are controls on the erodibility of coastal materials and the littoral sediment supply (Solomon 2005). Temporal variability is mainly controlled by environmental forcing (wind, waves, sea ice, currents, and sea level changes), thermal conditions and the presence of sea-ice (Solomon et al. 1994; Solomon 2005). The processes of shoreline recession and progradation are in response to these variations (Figure 1.3).

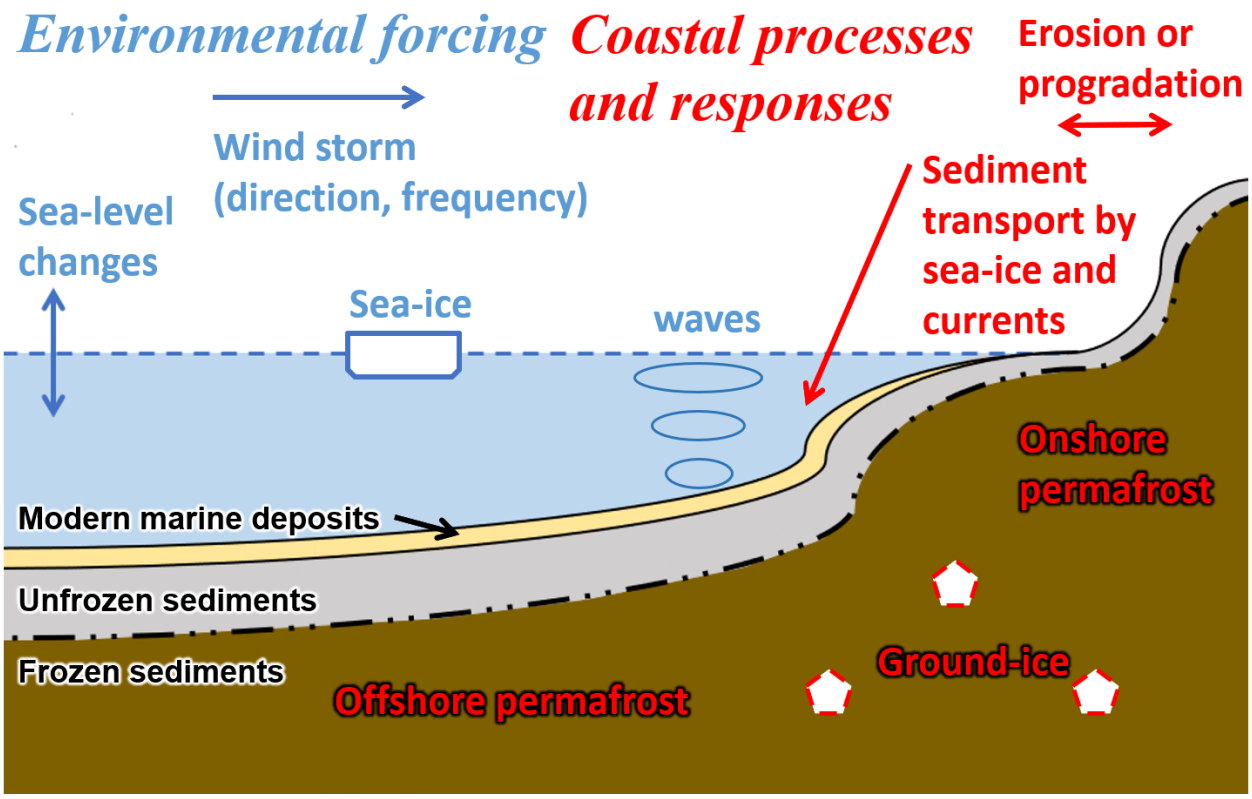

Figure 1.3: The environmental responses which lead to accelerated coastal erosion. (Modified from Rachold et al., 2005)

Sea level changes and the processes associated with waves and currents act together to modify the coast at temporal scales ranging from seconds to thousands and millions of years. As relative sea level rises it allows access of larger waves to the shore, which is why wave height and water surface elevation have been identified as one of the primary controls for coastal erosion (Wobus et al., 2011, Konopczak et al., 2014). Wave energy is dissipated through many mechanisms such as seafloor frictional drag and wave breaking (Lintern et al., 2013). Wave energy dissipation is an important component in nearshore coastal dynamics since it can re-suspend sediment in the nearshore region, allowing it to be subsequently transported by currents (Lintern et al. 2013).

Arctic coastal processes are strongly controlled by the presence and absence of sea ice, as it can act as a barrier protecting the coastline from environmental forcing (hydrodynamic forcing

and the thawing power of the warmer sea water) (Rachold et al. 2005, Manson et al. 2005). However, coastal erosion rates in the Arctic are comparable and even exceed temperate regions regardless of these restrictions (Rachold et al. 2000; Lantuit el al. 2013). The reduction in minimum sea ice extent due to a warming climate and the associated extension of the open water season is thought to affect the rate at which ice-rich unconsolidated coasts retreat (Lantuit et al. 2013, Wobus et al. 2011). The presence of longer open water seasons and increasing fetch from the coast to sea ice is predicted to increase wind induced waves (Lintern et al, 2013). Due to the threat of longer open water seasons and greater fetch, specifically in the fall, there has been a great deal of attention devoted to the impacts of storms on shallow coastal zones like that of the southern Beaufort Sea and other Arctic shelves (Lintern et al., 2013). Coastal regions tend to be heavily influenced by the impact of high magnitude weather events (Rachold et al. 2004). During the open water season storm winds can induce larger magnitude waves and surface currents (Hill and Nadeau, 1989). Storms in the Arctic are thought to be one of the largest drivers of coastal erosion (Overeem et al. 2011), although their influence is reduced by the presence of sea ice and terrestrial ice (permafrost and ground ice) (Atkinson 2005).

Unique to high latitude coastal regions is the presence of ground ice, which is known as all types of ice contained in freezing and frozen ground (Lantuit et al. 2011; Solomon 2005). The subaerial and subaqueous presence of ground ice is thought to be a major control on sediment budgets and nearshore morphological response (Mackay 1986; Wolfe et al. 1998; Dallimore et al. 1996; Mackay 1972). Ground ice can lead to thermal abrasion (TA), which is a process combining the kinetic action of waves and the thawing of ground ice (Are 1988). The process of melting ground ice enhances the vulnerability of the coastal zone to erosion. Coastal erosion is particularly enhanced by the thawing of massive ice (up to 80% ice) in coastal cliffs or the formation of

thermokarst features (Wolfe et al. 2001; Jorgenson & Brown 2005; Lantuit & Pollard 2005; Jones et al. 2008; Lantuit & Pollard 2008). Thawing-induced cliff top retreat (thermo-denudation) and marine abrasion (thermo-abrasion) are the two main erosional processes on Arctic coasts (Grigoriev & Rachold 2003). Thermo-denudation (TD) is when insolation and heat flux on coastal exposures thaws permafrost, leading to headwall erosion and the subsequent transport of material. Thermo-abrasion (TA) is the combined action of mechanical and thermal energy of sea water at water level causing erosion. Thermo-abrasion (TA) is only active during the open water season, while thermo-denudation (TD) can proceed throughout the summer. The intensities of these two coastal erosion processes (TA and TD) are controlled in part by the increasing of the open water season and the summer air temperatures (Grigoriev & Rachold 2003). In June as the air temperature rises and the snow melts, mud flows accumulate at the base of coastal bluffs while the adjacent sea is still covered in sea-ice (preventing TA). In late August TD rates slow since the coast refreezes, while TA can still occur until sea ice develops. Therefore, there is a phase shift between TA and TD. Based on results from Gunther et al. (2013) on Muostakh Island (Eastern Siberian shelf), the synchronicity of both TA and TD processes is more important than the extension of either active season.

1.4 Geomorphological features

Block failures (Figure 1.4) are an important component of coastal retreat in permafrost cliffs with semi-cohesive fine-grained sediments (Walker 1988; Williams & Smith 1989). Permafrost coasts are commonly characterized by the presence of ice-wedge polygons (Figure 1.5) (French 2007). Ice wedges are an important part of block failure erosional features since these

failures tend to occur along longitudinal axis of ice wedges which are oriented parallel to the coast (Figure 1.5) (Hoque & Pollard, 2016). Ice wedges are formed when temperatures fall below -15 ^{0}C as sediments and soil become brittle and crack. These cracks are then filled with meltwater come spring, and the meltwater is subsequently refrozen in these cracks creating an ice wedge. With each subsequent year ice wedges can grow due to the cracks expanding incrementally as meltwater freezes and expands, deepening and widening the size of the ice wedge and leading to more meltwater and more growth in subsequent years. A second important component in the formation of block failures is the formation of erosional niches at the base of cliffs (Hoque & Pollard, 2016). Through the process of thermo-abrasion, an erosional niche can be created, and as this niche extends into bluffs there are decreasing amounts of material underlying and supporting coastal bluffs, leading to the bluff failing and collapsing (Hoque & Pollard 2016). The mechanics of block failures are rather complex and still poorly understood due to a lack of data on niche geometry and the complexity of forces acting within frozen sediment due to the heterogeneous nature of ground ice (Hoque & Pollard 2016).

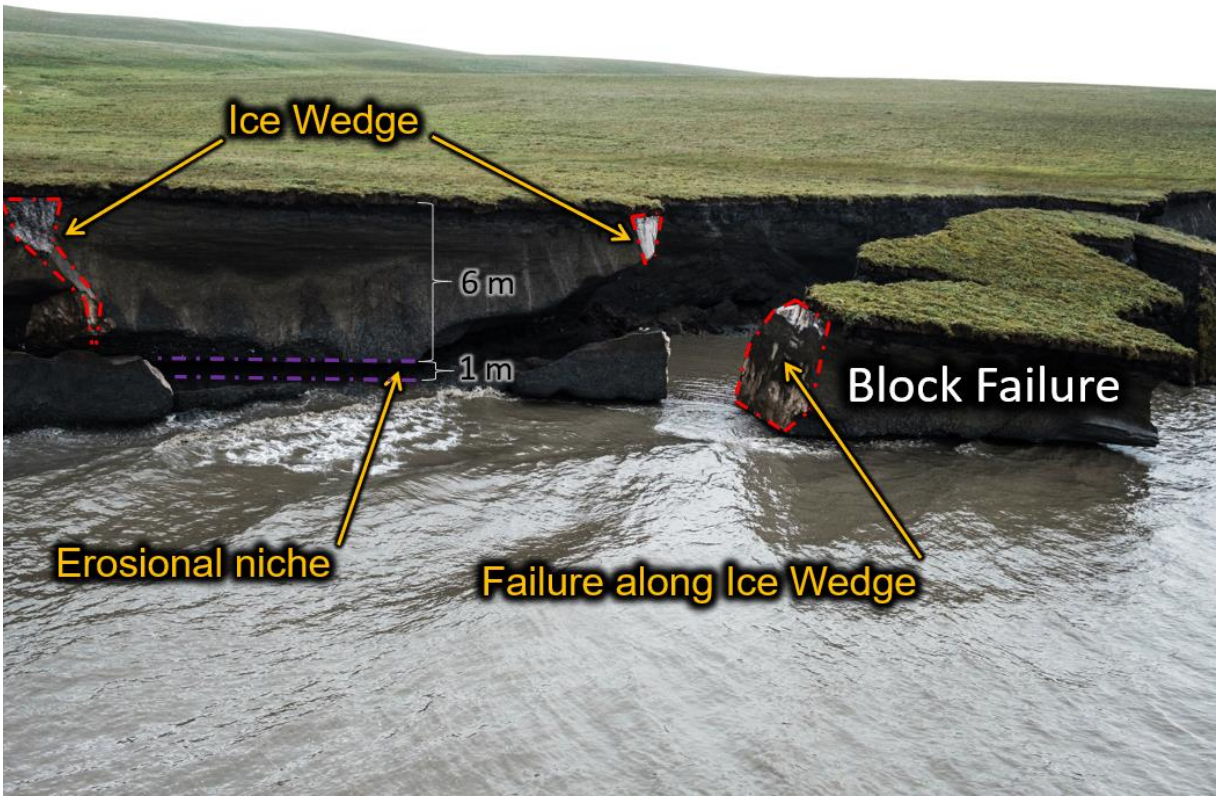

Figure 1.4: Block failures occurring on Pelly Island, NWT (August 2018 GSC expedition)

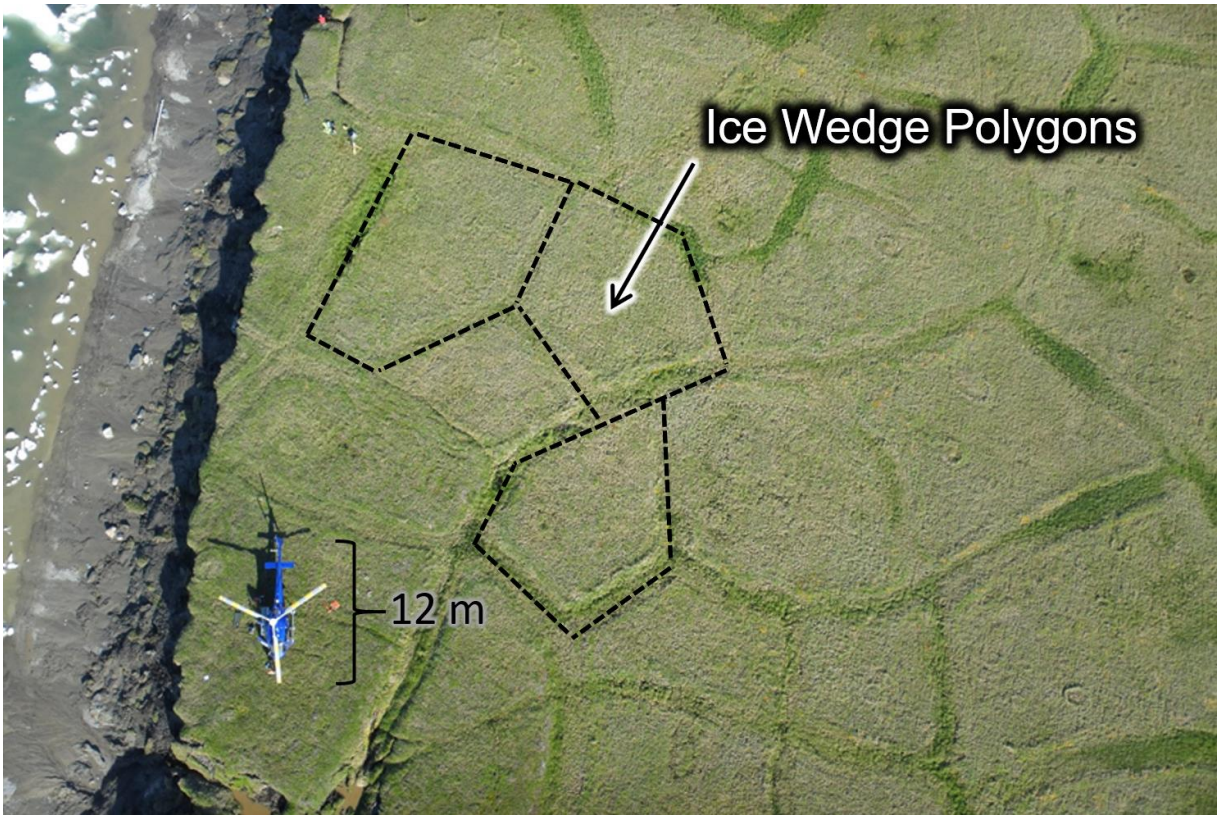

Figure 1.5: Ice wedge polygons on The Yukon Coastal Plain (July, 2018 NRCan/GSC expedition)

In many parts of the world, mainly temperate latitudes, former permafrost is indicated by ice wedge casts (Figure 1.6) (Péwé, Church, and Andresen 1969). Ice wedge casts are formed when ice wedges are thawed due to lowering of the permafrost table allowing water carrying sediment to percolate down into the polygonal trenches. As the sediments surrounding the polygonal trenches lose their cementing ability due to thawing ice, sediments collapse into the area formally occupied by the ice wedge and are preserved as an Ice wedge cast. Ice wedge casts are widely used as palaotemperature indicators (Murton, Péwé 1966 a,b).

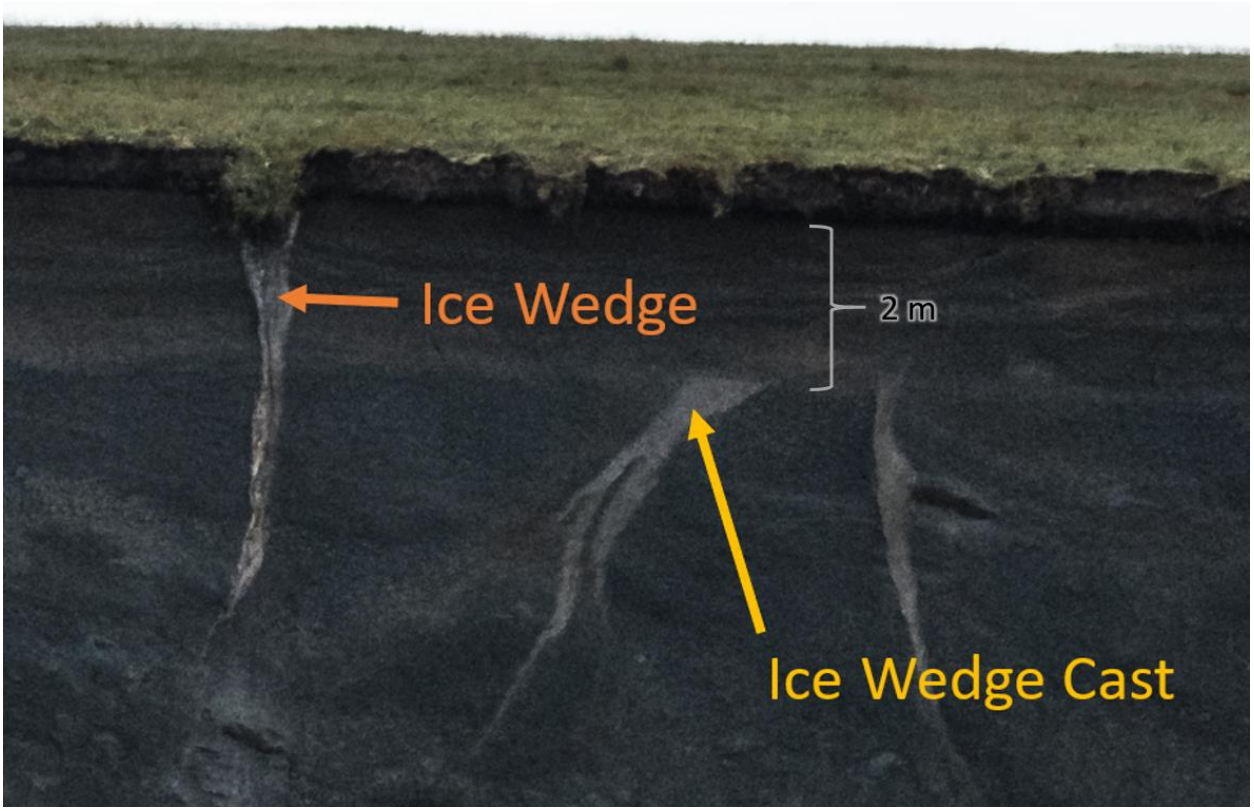

Figure 1.6: An Ice wedge cast in comparison to an active ice wedge (August 2018 GSC field season)

The Beaufort Sea coast is the most ice-rich permafrost coast in the Canadian Arctic and experiences high rates of erosion and retrogressive slump activity (Figure 1.7) (Lantuit & Pollard, 2008). Thermokarst is defined by van Everdingen 1998 as the process which drives landform characteristics resulting from the thawing of ice-rich permafrost and/or melting of massive ice.

Retrogressive thaw slumps are closely linked to coastal processes, as they are often initiated by wave erosion at the base of coasts uncovering massive ice (Burn & Lewkowicz 1990). Thaw slumps are often initiated by thermo-abrasion at the base of coast bluffs uncovering massive ice, thawing of exposed ground ice leads to a retreating slope face creating retrogressive slumps (Lantuit & Pollard, 2008; de Krom 1990). If massive ice melts at a rate faster than coastal erosion, thaw slumps form (Lewkowicz, 1987). The formation and magnitude of thermokarst features is directly connected to the thermal stability of the upper section of permafrost and the ground-ice content (Lantuit & Pollard, 2008).

Figure 1.7: Thaw slump along the Canadian Beaufort Sea coast (photo by: Roger Macloed/ 2016 GSC)

1.5 Spatial and Volumetric change analysis

Terrain models derived from unmanned aerial vehicles (UAVs) and structure from motion software (SfM) have demonstrated the ability to produce high resolution digital surface models

with the precise geographic positioning necessary for GIS based volumetric change measurement (Haas et al. 2016). Accurate and high-resolution terrain models are essential so that geomorphic features may be accurately represented and their change over time accurately quantified. Digital Surface Models (DSMs) are a 3D representation of a surface which are created from elevation data and include elevation values from objects on the surface of the earth such as houses or trees, whereas Digital Elevation Models (DEMs) represent the surface of the earth excluding objects on its surface (https://desktop.arcgis.com/en/arcmap/10.3/manage-data). A DSM can be in raster or vector format, with the raster datasets being composed of square cells in a grid and vector datasets being composed of a triangular irregular network (TIN). DSMs are most commonly created using elevation data collected using remote sensing (photogrammetry, lidar, InSAR) but they can also be created from land surveying. Recent advances in ground-based, airborne-based, and remotely sensed survey methods, such as structure from motion (SfM) and light detection and ranging (LiDAR), have revolutionized the collection of high-resolution terrain models. The use of unmanned aerial vehicles (UAVs) coupled with the photogrammetric method of SfM can be significantly more cost effective compared to LiDAR when surveying smaller parcels of land, which has contributed to its widespread adoption for budget research applications across a range of scientific disciplines (Eltner et al. 2016; Westoby et al. 2012). Auto-pilot systems integrated in UAV applications have also increased the ease of use while high quality digital cameras and GPS have enabled UAVs to collect high resolution imagery with precise geographic positioning (Turner et al. 2015). This thesis uses UAVs and the SfM method to analyze the volumetric erosion for the northwest cliffs (NW) of Pelly Island annually between 2016 and 2019.

Previous research on the historical (1972 to 2000) shoreline change rates in the Beaufort Mackenzie region was conducted by Solomon (2005), who reported the mean shoreline change

rate using Digital Shoreline Analysis System (DSAS) (Thieler et al., 2009). The research presented in this thesis uses Analyzing Moving Boundaries Using R (AMBUR) (Jackson 2009) as the approach for 2D shoreline change analysis of Pelly Island. The combination of AMBUR with high resolution satellite imagery is expected to provide accurate and up-to-date assessment of coastal erosion rates between 1950 and 2018. The influence of surface geology and shoreline orientation are also analyzed to identify possible controls on shoreline change.

Both human and biological systems in the nearshore and offshore environments can be altered by changes in the coastal zone. In the past two decades there has been an acceleration of erosion of ice-rich permafrost in the Arctic due to changing environmental factors such as declining sea ice, warming temperatures and increased forcing events (Lantuit et al. 2012, Khon et al. 2014, Johannssen et al. 2002, Manson et al. 2005). Our research seeks to provide a better understanding of the coastal change occurring on Pelly Island, which lies within the ecologically and biologically significant Okeevik MPA (Integrated Ocean Management Plan for the Beaufort Sea 2003) and hopes to provide an updated assessment of coastal response to changing external conditions. More specifically our research leverages advances in technology and analysis techniques to accurately determine short-term volumetric erosion rates and long-term planimetric erosion rates and the influence of surficial geology and storminess on these processes.

The purpose of this study is to determine the controls on shoreline change rates for Pelly Island from 1950 to 2018. The primary objective is to examine the influence of surficial geology and exposure on shoreline rates. The second objective is to compare our estimates of shoreline change rates to the previously documented values (Solomon 2005).

Chapter 2: Study Area

The landscape of the Mackenzie Beaufort region was formed by recurring glaciations and varying sea level of more than 140 m below present sea level (Hill et al, 1985). Over the past ten thousand years the Mackenzie Delta has prograded into the Beaufort Sea (Hill et al., 2001) depositing deltaic sediments between Pleistocene uplands at the mouths of Mackenzie River distributary channels (Figure 1.1). Pelly Island is part of these Pleistocene upland deposits, which have been altered by glacial, marine, fluvial, and coastal processes. The region became ice-free approximately 20,000 yr BP (Tuktoyaktuk uplift rate of 1.04 $m \cdot a^{-1}$ from James et. al. 2014) is experiencing relatively minor isostatic uplift (compared to the Canadian Shield) and an ongoing marine transgression (average sea level change of 1.7 $cm \cdot a^{-1}$, RCP 8.5 Projection at 2010 from James et. al. 2014) (Lantuit et al. 2013; Konopczak et al. 2014; Hill et al, 1985). The hummocky uplands of Pelly Island are composed of surficial moraine deposits and lacustrine deposits. Moraine deposits consist of till, forming a veneer generally less then 1 m thick, and are assigned to the Toker Point Member of the Tuktoyaktuk Formation. Underlying the moraine deposits are pre-Wisconsin aged units, composed of glacial materials deposited during the early Toker Point Stade (Rampton 1988). They can be identified by the unconformity between the Kidluit formation and the Kittigazuit formation (Figure 2.1). In low lying thermokarst basins, surficial lacustrine deposits take the form of drained lake beds, which are generally two to eight metres thick and composed of a reworked matrix of the surrounding glacial materials (Murton 2009, Rampton 1988). Abundant sediment supplied from both the Mackenzie River and coastal erosion has led to the development of Holocene marine deposits in the form of wide beaches, extensive spits, and barrier islands.

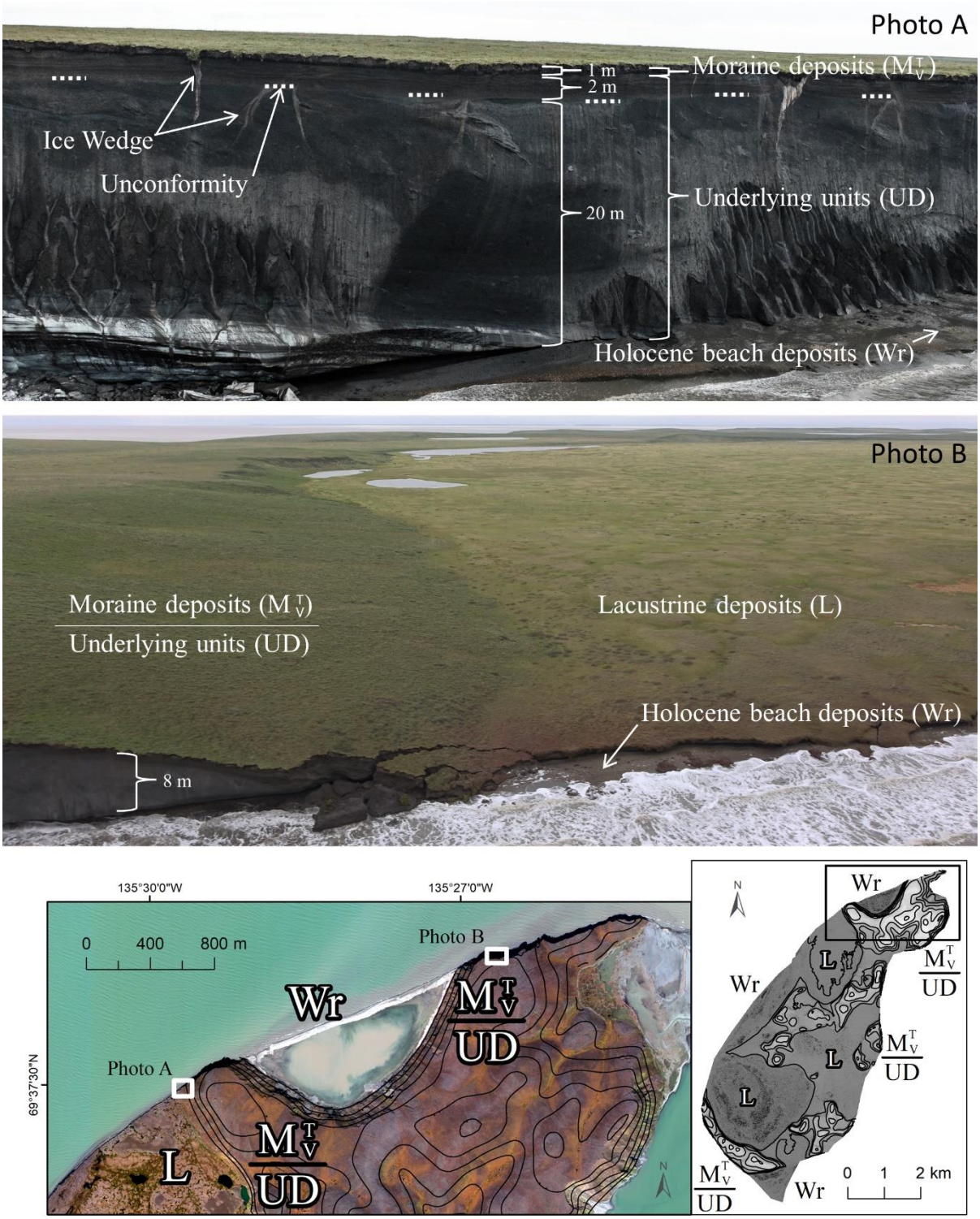

Figure 2.1: Surficial geology of Pelly Island comprises moraine deposits (M_v^t), underlying units (UD), lacustrine deposits (L), Holocene beach deposits (Wr). Photo A and B were taken along the northwest cliffs of Pelly Island (August 2018 and 2019 GSC field season). Locator map (bottom left) background is 2013 Geoeye-1, inset map (bottom right) background is a 2013 digital elevation model (DEM) courtesy of Porter et al., 2018, "ArcticDEM". Both locator and inset map include 5 m contour lines derived from the 2013 DEM.

2.1 Coastal processes in the Canadian Beaufort Sea

Sea-ice cover in the Beaufort Sea is about seven to nine months long (Melling et al., 2005; O'Brien et al., 2006; Lintern et al. 2013), acting as a physical barrier restricting erosion from hydrodynamic forcing and thawing of permafrost due to the access to warmer sea water (Rachold et al. 2005). Open-water conditions in the Beaufort Sea are mainly characterized by wind-driven waves, and with the presence of longer open water seasons and increasing fetch from the coast to sea ice, it is predicted that wind induced waves are to increase in magnitude (Lintern et al, 2013). Storm winds in the Beaufort Sea have been known to reach over 80 $km \cdot h^{-1}$ (Hill and Nadeau, 1989). Manson and Solomon (2007) predict that the overall relation between magnitude and frequency of storms may change in the Beaufort Sea, with the frequency predicted to decrease slightly and the magnitude of storms to increase along with flood risk. Pelly Island and adjacent areas are undergoing rapid rates of erosion and accretion which are driven by periodic storms and long-term sea level rise (Solomon 2005). Manson et al (2005) identified coastal morphology, sea-level trends, sea ice, and storms as the major controls on spatial variability in the Canadian Beaufort Sea

2.2 Coastal features in the Canadian Beaufort Sea

The Canadian Beaufort Sea is known to be quite shallow, both in the nearshore region and extending out towards the slope of the continental shelf, with the distance to the 10 m isobath being over 10 km from Pelly Island's shoreline (Lintern et al, 2013). Coastal landscapes in the area are composed of hummocky till-capped hills and organic-rich drained lakes beds (Rampton 1988; Dallimore et al, 1996; Murton et al. 1997). Most of the region is composed of poorly bonded

sediments which are relatively easily resuspended by waves and transported by currents (Lintern et al., 2013). The Beaufort Sea is known to have large sediment fluxes which are dominated by sediment discharge from the Mackenzie River (Hill and Nadeau 1989; Macdonald et al., 1998). Abundant sediment supply from coastal erosion has formed wide beaches and extensive spits from exposed headlands, some of which have detached from their headland sources and turned into barrier islands (Figure 2.2). Beach and nearshore profiles are characterized by a relatively steep slope from the water line flattening out at about 3-4 m depth (Solomon 2003).

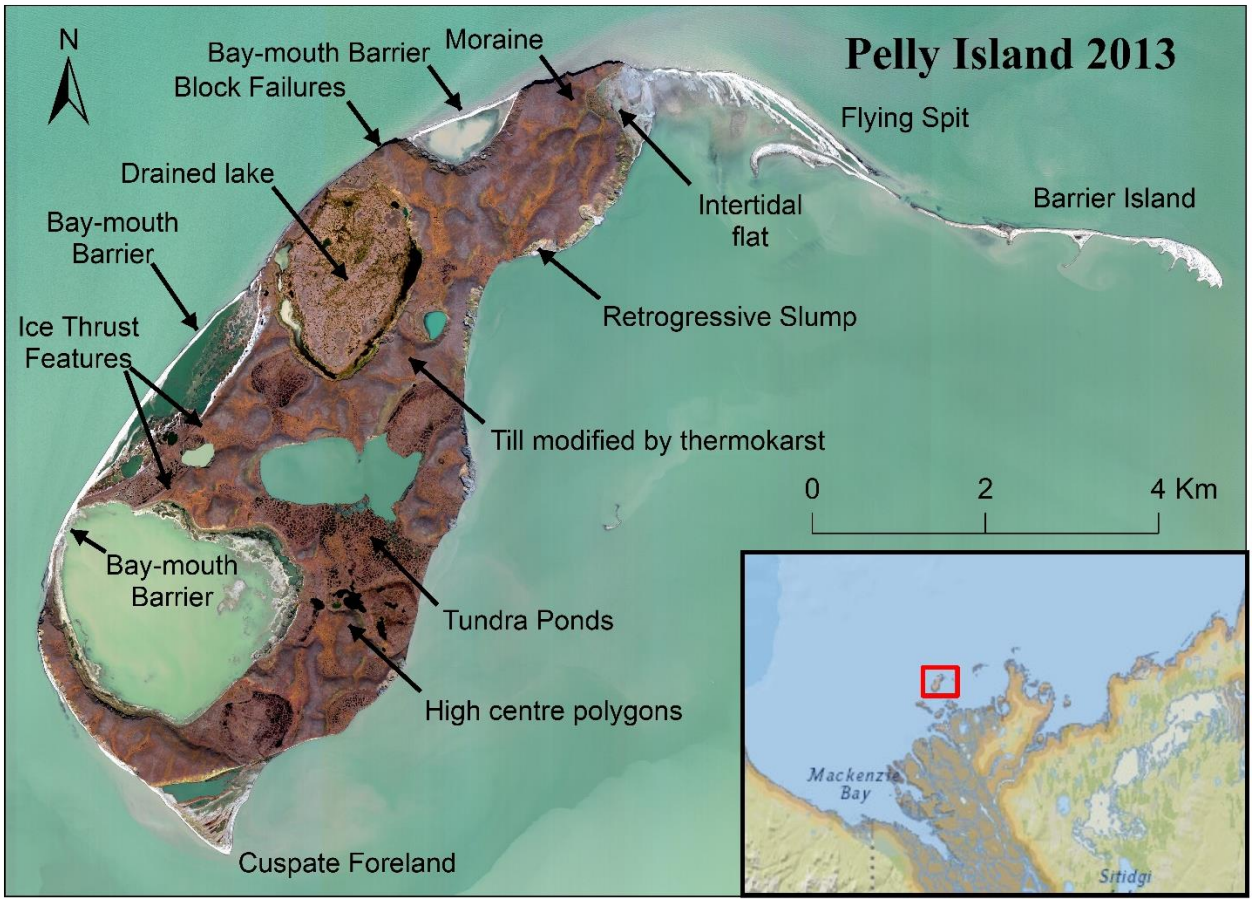

Figure 2.2: A geomorphic description of Pelly Island in 2013 (Geoeye 2013)

Chapter 3: Methods

Coastal change was assessed using four UAV surveys between year 2016 and 2019 to improve the understanding of the quantity of sediment delivered to the nearshore of Pelly Island. Air photos and satellite imagery collected between years 1950 and 2018 were also used to calculate rates of shoreline change and the influence of surficial geology on these changes.

3.1 Volumetric Analysis

To better understand the rapid changes occurring on Pelly Island we have conducted a volumetric analysis of sediment resulting from erosion of the northwest cliff on an annual basis using DSMs created from aerial photogrammetry, which were acquired using UAVs during field surveys between 2016 and 2019. Software using SfM processing was used to create 3D models of the coastal cliffs from 2D low altitude, hyperspatial aerial photos. Estimated ground ice concentrations formulated by Dallimore et al. (1996) on Richards Island were used to estimate ground ice concentration on the NW cliff of Pelly Island. The morainal deposits found on the outer islands (Pelly Island, Garry Island, Kendal Island) of the Mackenzie Delta are described as being of similar geological origin and composition to that of Richards Island (Rampton 1987). By calculating the volume change between DSMs from 2016 to 2019 and subtracting the estimated ground ice concentrations, it was possible to estimate the volume of sediment delivered to the nearshore from the NW cliff during this time period.

3.1.1 Change Detection using UAV-SfM

A total of four annual UAV surveys were conducted in 2016, 2017, 2018, and 2019 between the months of July and August along Pelly Island's NW cliff. A base station was established to collect a GPS coordinate on a known point using a Real Time Kinematic Differential Global Positioning System (RTK DGPS). The base station was then able to provide accurate corrections of 3D points collected by the RTK rover, which sends the position of a point collected to the base station for corrections. The 3D points were collected in the center of square colored targets which were used as Ground Control Points (GCPs) (Figure 3.1). Each GCP was surveyed to collect their respective geospatial position using a Hemisphere S321 multi-GNSS, multi-frequency smart antenna receiver (Figure 3.1). The targets were placed strategically along the top and bottom of the North West cliff in a zig zag pattern and in each corner of the survey area at approximately 200m apart ensuring adequate spacing between GCPs (Tonkin and Midgely, 2016). This was done following the evolving recommendations found in the literature focusing on using UAVs and SfM for change detection in various landscapes (Tonkin and Midgely, 2016; Raczynski, 2017), using a minimum of 4 GCPs (actual range 10-22) for georeferencing with the remaining used as check points for the accuracy of georectification when available (Tonkin and Midgely, 2016). The DGPS rover received RTK corrections via its base station which had corrected its logged position for over three hours. These positions were then corrected using Precise Point Positioning (PPP). The reported horizontal and vertical accuracies for the S321 are 20 mm and 40 mm respectively (https://www.hemispheregnss.com, 2020), however it yielded accuracies of approximately 1 cm in the horizontal and 1-3 cm in vertical. The GCPs were surveyed in the NAD83 CSRS UTM Zone 8 Epoch 2010 coordinate system. The vertical datum was CGVD28.

These coordinates were converted to CGVD 2013 using GPS H 3.3 software (https://webapp.geod.nrcan.gc.ca/geod/tools-outils/gpsh.php?locale=en).

Figure 3.1: A Hemisphere S321 RTK rover being used to collect a GPS point on a GCP on Pelly Islands (August 2018, GSC)

The UAVs used for aerial surveys were: DJI Phantom 3 Professional in 2016 and 2017; DJI Phantom 4 Professional in 2018 (Figure 3.2); and a DJI Mavic 2 in 2019. All surveys were flown with the *Pix4D Capture App* in 2016 and 2017, and the *DJI Ground Station Pro App* in 2018 and 2019. UAV Surveys were conducted with approximately 50 m of altitude with a speed of approximately 2 to 3 $m \cdot s^{-1}$. The pictures used in the SfM software were nadir facing and had between 65% and 80% sidelap and 75% and 85% frontlap. The resultant pixel size of the DSM was approximately 2 cm (1.9-2 cm).

Figure 3.2: Conducting a UAV survey of Pelly Island's using a DJI Phantom 4 Professional (August 2018, GSC)

Digital Surface Models (DSMs) were created using aerial imagery of Pelly Island's northwest cliff. Data files were imported into the structure from motion software *Pix4d* to stitch together tie points found from overlapping 2D images using algorithms to create DSMs. These 3D terrain models, or DSMs, were then georeferenced in *Pix4d* by assigning ground control points to their respective geographic position. Pix4D workflow utilizes a variation of SfM-MVS workflow described above (Carrivick et al, 2016; pix4d.com, 2020). The default settings were used for the Initial Settings, the Point Cloud and Mesh creation and the DSM orthomosaic creation. The value used for the Horizontal and Vertical Accuracy columns in the GCP Manager was the accuracy reported by the RTK DGPS associated with the GCP (2 cm). Once the DSMs were created, they were exported and further processed using the GIS software package *ArcGIS 10.6* (Figure 3.3).

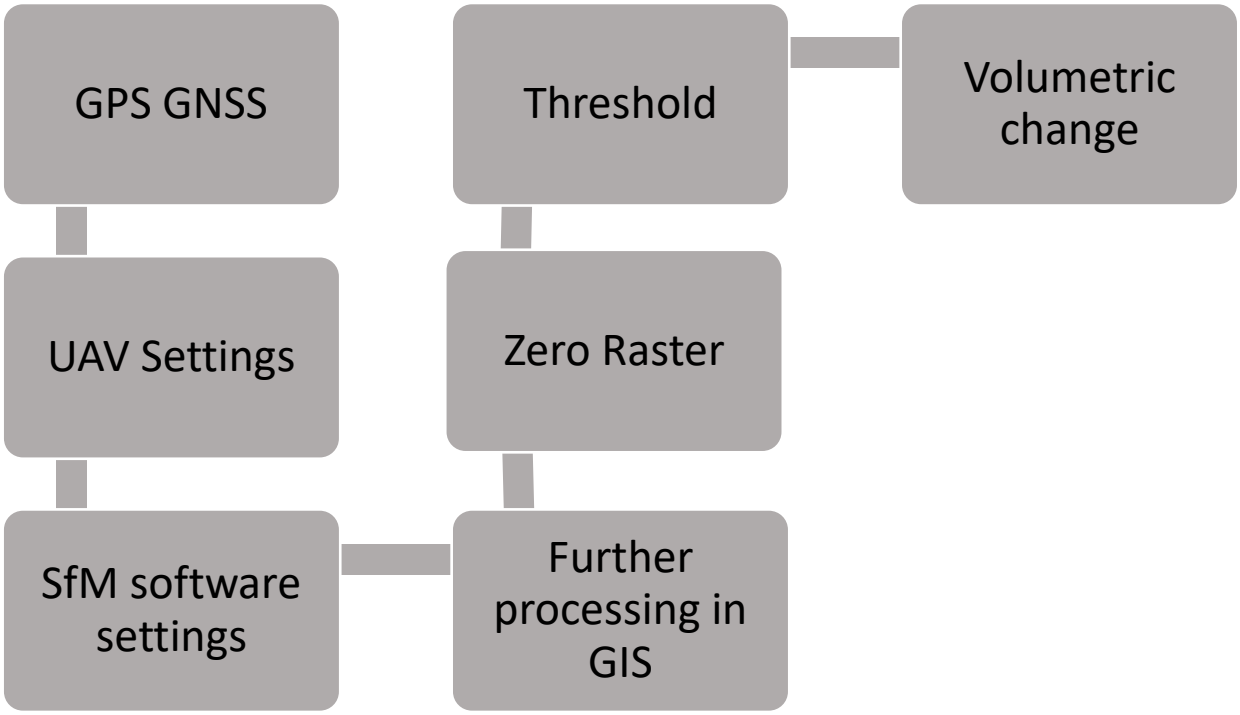

Figure 3.3: Workflow for Pelly Island's Volumetric change of the NW cliff from 2016-2019

To obtain an accurate estimate of volumetric change of the NW cliff it was important to remove any areas of the DSM which negatively influenced the accuracy of the analysis (Haas et al, 2016). This meant removing any artifacts which give an over-estimation of surface elevations in the DSMs when there is not an adequate number of tie points to perform a quality bundle adjustment. A hillshade visualization was applied to the DSMs to identify artifacts which were subsequently removed using the clip tool. Artifacts created in the DSMs due to ocean waves were removed (Figure 3.4), and a few meters of the perimeter of each DSM were removed where artifacts created from GCPs were found to not properly calibrate with the point cloud in *Pix4d*.

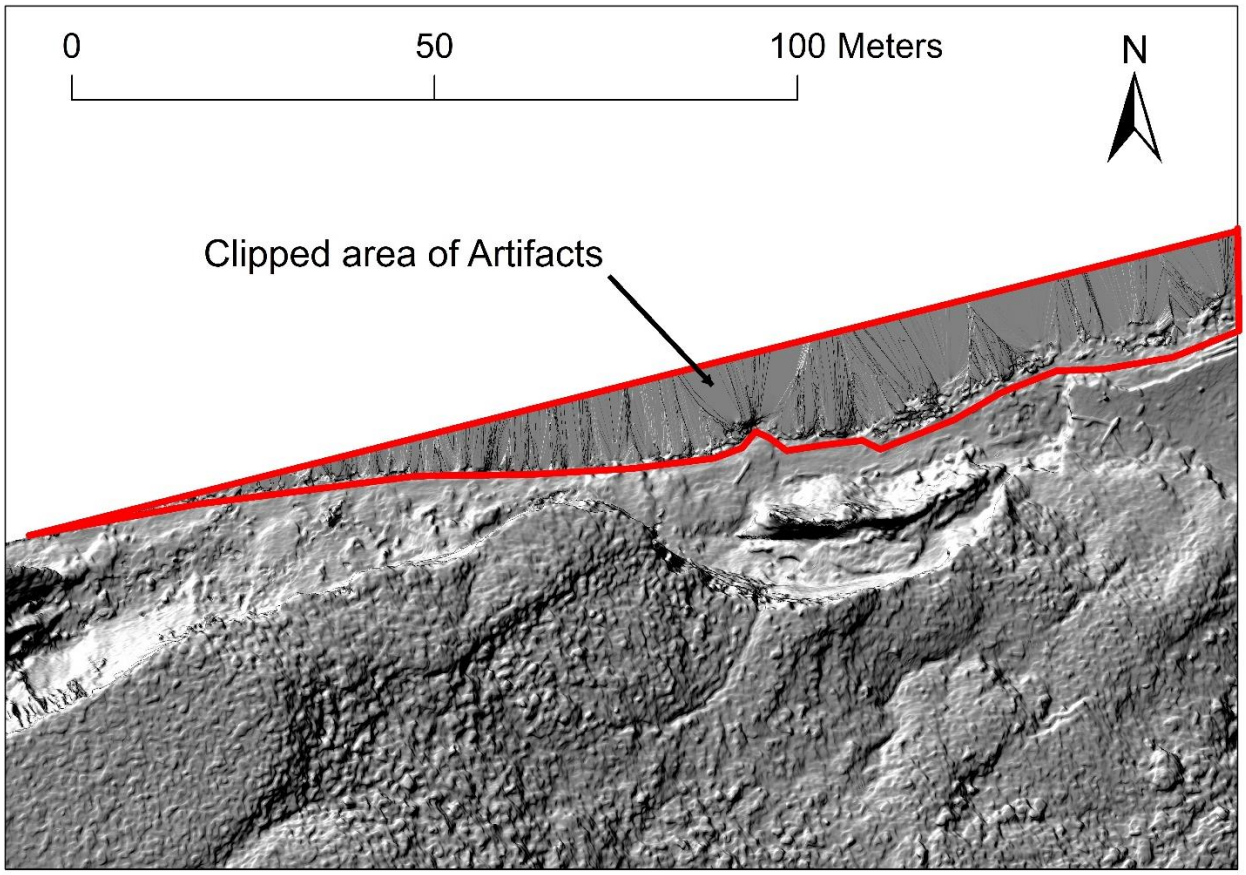

Figure 3.4: A clipped area of artifacts in the 2019 DSM created by the presence of water.

3.1.2 Volumetric Change

A sequence of calculations was conducted using *ArcGIS 10.5* to measure the amount of sediment which was eroded and subsequently deposited into the nearshore from summer 2016 to summer 2019. To prepare the DSMs for volumetric analysis, each DSM was clipped to ensure they had the same geographic extent. The *Difference Function* was then used to create four new rasters representing the difference in elevation at each pixel between the 2016 and 2017 DSMs, the 2017 and 2018 DSMs, the 2018 and 2019 DSMs, and finally the 2016 and 2019 DSMs. A Level of Detection (LoD) threshold was applied to each difference raster to ensure that only the pixels

which underwent significant changes in elevation between the two DSMs are used for calculating volumetric change. The LoD threshold was determined using Equation 1 (Wheaton et al., 2010):

$$U_{crit} = t(\delta DoD) \quad (1)$$

where *t* is equal to 2.807 (for a 99.5% confidence interval) and is multiplied by the uncertainty between the two DSMs (Wheaton et al, 2010), which is found using Equation 2:

$$\delta DoD = \sqrt{(RMSE_{ZOld})^2 + (RMSE_{ZNew})^2} \quad (2)$$

where $RMSE_{zOld}$ is the root mean square error value of the vertical component of the older DSM, and $RMSE_{zNew}$ is the root mean square error value of the vertical component of the newer DSM (Brasington et al., 2003; Lane et al., 2003). The error of each DSM was reported as a root mean square error value ($RMSE_Z$) of the vertical component of the DSMs, which were obtained using check points from RTK-GPS measurements and comparing measured values with those in the DSMs (Smith and Vericat, 2015). In cases where $RMSE_z$ could not be calculated due to lack of check points, the error for the DSM was reported by multiplying the pixel size of the DSM by three (pix4d.com, 2020).

Once a LoD threshold was determined using Equation 1, raster calculator was used to set all values within the LoD threshold to be No Data for each respective DEM of Difference. All pixels with positive elevation change (growth) were also set to No Data since we are only interested in finding the volume loss over time. Volume change was then calculated using the *Cut Fill* tool in ArcGIS, which calculates volume changes by using the elevation at each pixel between the two DSMs and multiplying it by the area of a pixel where *c* equals pixel size in equation 3:

$$\sum[(DSM_{new} - DSM_{old})\, c^2] \quad (3)$$

3.2 Spatial and Temporal Variability of Shoreline Change

3.2.1 Air photo and satellite image acquisition

Air photos of Pelly Island were acquired from the National Air photo Library for years 1950, 1972, 1985, and 2000 and were scanned at 400 dpi to produce digital images (Table 1). Satellite imagery was obtained for the years 2013 (Geoeye-1), and 2018 (Sentinel-2). All imagery was co-registered to an orthorectified 2013 Geoeye-1 satellite image of Pelly Island in the NAD83 CSRS UTM Zone 8 Epoch 2010 coordinate system with all root mean square (RMS) error values below 6.0 m.

3.2.2 Uncertainty of shoreline position

The imagery was then enlarged to the 1:1000 scale to digitize Pelly Island's shoreline, with the water line used as the shoreline proxy and when not visible the cliff top was used (Figure 3.5). Due to the inherent high variability of shoreline position of the Pelly Island spit, it was excluded from the analysis as per the Solomon (2005) study. Positional uncertainties were calculated for each digitized shoreline to account for errors in the co-registration process along with variations in spatial resolution. The uncertainty of each shoreline position (U) was calculated using equation (4) (modified from Hapke and Reid, 2007):

$$U = \sqrt{(E^2_{GR\ aligned\ image} + E^2_{GR\ master\ image} + RMS^2 + LOA^2)} \qquad (4)$$

where, $E_{GR\ aligned\ image}$ is the ground resolution of the source image, $E_{GR\ master\ image}$ is the ground resolution of the 2013 orthorectified Geoeye-1 satellite image, RMS is the root mean square error of the ground control points (GCPs) used in the georectification process, LOA is the loss of accuracy created by the user while digitizing (from Hapke and Reid, 2007). The positional

uncertainty for each shoreline ranged between a low of 2.7 m for the 2013 GeoEye-1 shoreline to a high of 10.5 m for 2018 Sentinel-2 shoreline (Table 1).

Table 1: Metadata and accuracy for remote sensing imagery of Pelly Island 1950-2018.

Date	**Number of images**	**Type of image**	**Scale 1 to**	**Ground resolution**	**Ground control points (GCP)**	**Root mean square (m) 2nd order Polynomial**	**Loss of accuracy (LOA) (m)**	**Uncertainty (m)**
2018	1	Sentinel-2 L1C (multispectral)	/	10	9	1.89	2	10.5
2013	1	GeoEye-1 (multispectral)	/	1.8	Base image	/	2	2.7
2000	2	Polychrome air photos	58 000	3	21	1.79 to 3.67	4	6.5
1985	1	Monochrome air photos	60 000	3	15	3.4	4	6.3
1972	2	Monochrome air photos	60 000	3	17	0.62 to 5.24	4	7.4
1950	2	Monochrome air photos	40 000	2	22	2.03 to 5.84	3	7.1

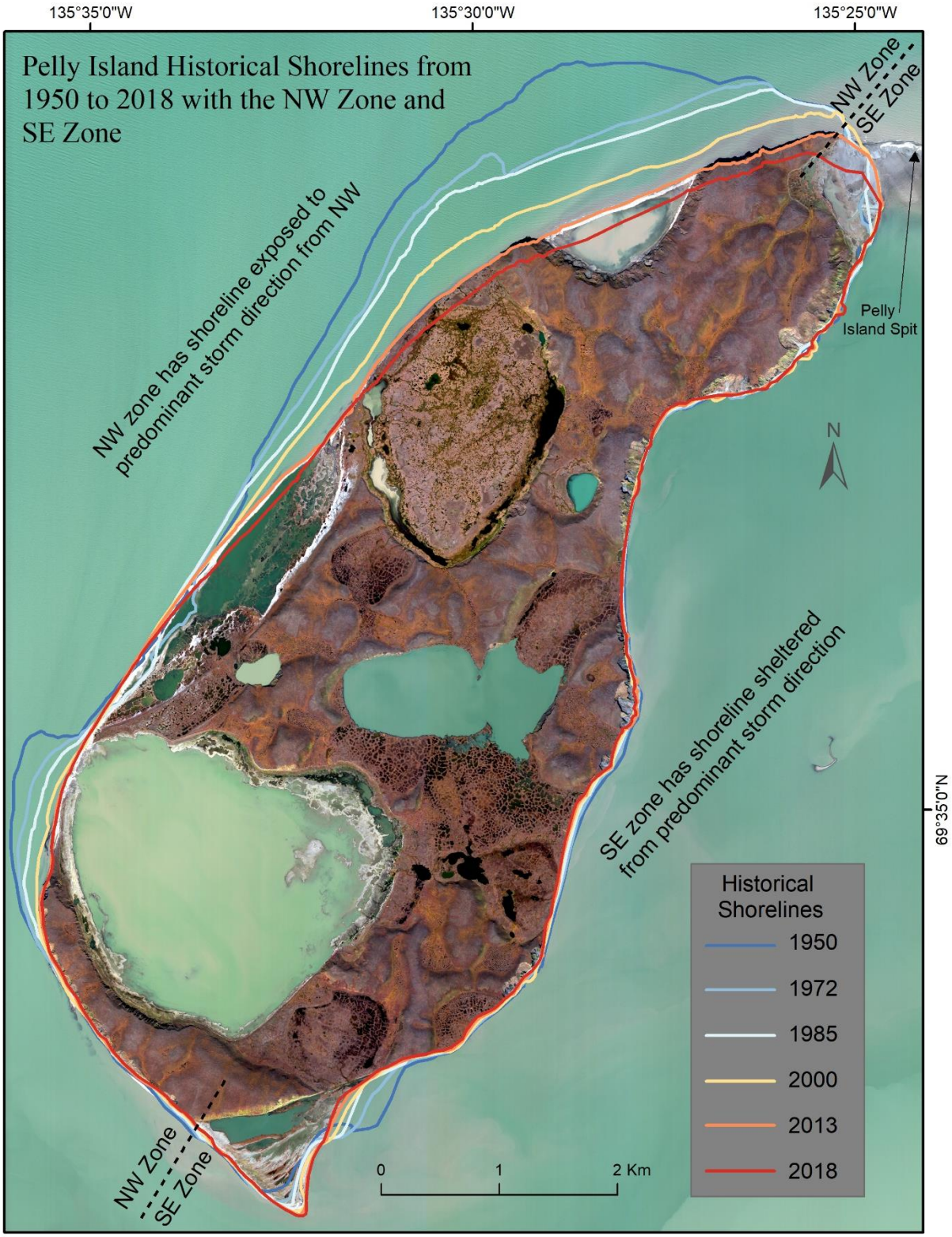

Figure 3.5: Digitized historical shorelines of Pelly Island for years 1950, 1972, 1985, 2000, 2013, and 2018. Also shown is the designated NW zone, facing the predominant storm direction, and the more sheltered SE zone of the island. Background is a 2013 GeoEye-1 satellite image.

3.2.3 Shoreline change analysis

Shoreline position changes were analyzed and visualized using AMBUR (Analyzing Moving Boundaries Using R) (Jackson 2009) to quantify distances and rates of shoreline movement. The measured change was reported as End Point Rate (EPR), which is the rate of change between shorelines from two time periods measured along a transect. The measured change was also reported as a Linear Regression Rate (LRR) for all historical shorelines digitized between 1950 and 2018. In total, the EPR and LRR were calculated along 550 transects.

In AMBUR the shoreline movements were calculated between inner and outer baseline vectors (baseline was drawn offshore of the historical shorelines, and an inner baseline located onshore) using the 1950 and 2018 coastlines. Transects were cast perpendicular to the coast, between the two baselines, at 50 m intervals. Rates of shoreline change were calculated for each transect intersection using the end-point rate (EPR) formula. The shoreline change summary statistics net, minimum, maximum, mean, and standard deviation were then calculated for each transect and for each observation period. All computed AMBUR shoreline change rates are published in a comma-separated value file in the supplemental information database (*Pelly_Supertable.xls*). The EPR was calculated using the following equation:

$$EPR = \frac{D_2 - D_1}{T_2 - T_1} \qquad (5)$$

where, *D* is the distance between historical shoreline points along a transect and *T* is the year the image was obtained. Using the positional uncertainty (U) values from Equation 4, the Dissolution of Accuracy (DOA) for each observation period was calculated using equation (6) (equation modified from Foster and Savage, 1989):

$$DOA = \frac{\sqrt{U_1^2 + U_2^2}}{\Delta T} \quad (6)$$

where, U_1 is the uncertainty of shoreline position from the first point in time, U_2 is the uncertainty of shoreline position from the second point in time, and ΔT is the time duration, in years between the digitized shoreline source images. These DOA values are shown in Table 2. Significant changes in shoreline change rates using EPR were identified as those that exceeded a two-sigma deviation from the mean change rate *(Pelly_Supertable.xls)*. The two-sigma (2σ) changes were calculated using the mean EPR and standard deviation of each transect using equation (7), with n being the number of transects:

$$\frac{\sum EPR_n}{n} \pm 2\sigma \quad (7)$$

A linear regression (LRR) analysis was also conducted, and the standard error of the coefficients of the linear regression calculated using the P value (equal or less than 0.5) of the linear regression.

Table 2: The Dissolution of Accuracy (DOA) for shoreline positions for each observation period.

Time Period	**DoA(m·a^{-1})**
1950 to 1972	0.5
1972 to 1985	0.7
1985 to 2000	0.6
2000 to 2013	0.5
2013 to 2018	2.1
2000 to 2018	0.7
1950 to 2018	0.9

3.2.4 Coastal exposure

To examine the relationship between coastal exposure and predominant storm direction on shoreline change, Pelly Island was divided into two zones: one facing the predominant storm direction from the northwest (NW Zone) (Hill et al., 1991; Lintern et al., 2013; Solomon 2005, Manson and Solomon 2007), and the other facing the more sheltered Southeast (SE zone) (Figure 3.5).

Records of historical wind speeds and direction were obtained from Environment Canada's online climate data archives (http://climate.weather.gc.ca) for a weather station on Pelly Island (weather station number 2203095) to better understand the influence of storms on erosion during the open water season. A database of hourly wind speed and direction was created; however, data were only available for download between years 2005 to 2018 (see supplemental data Pelly_Island_Historical_Wind.xls). In order supplement our storm database we included the storm count from the 2007 Manson and Solomon study, which had access to wind data from the weather station on Pelly Island from 1994 to 2000, and combined it with data from three wind stations in Tuktoyaktuk from 1958 to 2000 to create a synthetic wind record of Pelly Island from 1958 to 2000. To keep as much consistency between Manson and Solomon's (2007) record of storms from 1958 to 2000 with our 2005 to 2018 storm record we defined storms using the same criteria., Storms were identified during the open-water season (June to October) and defined as events with wind speeds greater than 50 $km \cdot h^{-1}$ for at least six hours with a wind vector cut off which only included winds from the north-westerly direction (270° to 360°). The storm count for each observation period can be found in Figure 3.6.

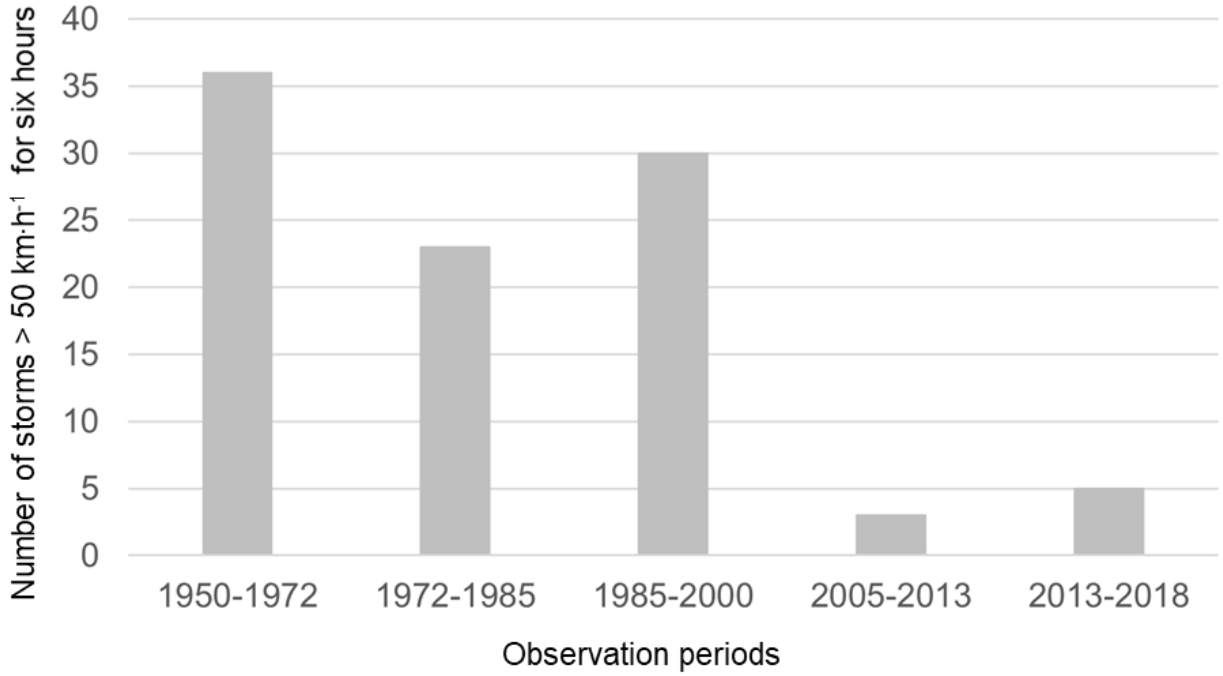

Figure 3.6: A record of storms on Pelly Island from 2005 to 2018 merged with a synthetic record of storms from 1950 to 2000 sourced from Manson and Solomon (2007). Storms were defined by at least six hours of wind speeds greater than 50 km·h^{-1} with a wind vector cut off which only included winds from the north-westerly direction (270° to 360°) during the open-water season (June to October).

3.2.5 Classification of Surficial Geology

To investigate the role of surficial geology on shoreline change rates, a surficial geology classification was created by modifying Rampton's 1987 surficial geology map of Pelly Island to identify general location of the three surficial geology deposit types shown in Figure 1.1 (Geological Survey of Canada Map 1647A, Rampton, 1987). The map was then refined utilizing the air photos based on geomorphological characteristics. Beaches and barrier islands were classified as Holocene marine deposits, lower lying headlands that appear to be drained lake beds were mapped as lacustrine deposits, and all other headlands were classified as moraine deposits. The same method was applied using the 2013 and 2018 satellite imagery with the addition of a 2013 and 2018 2 m digital surface model (Porter et al., 2018, "ArcticDEM") used to identify lower

elevation drained lake beds as lacustrine deposits. We used our modified surface geology mapping to classify each of the digitized shorelines to examine the relationship between surficial geology and the spatial and temporal variability of shoreline change. This was done using a multistep spatial attribute query to identify transects which cross the same surficial geology units within subsequent shoreline years. The identified transects were then matched to corresponding EPR results (Figure 3.7).

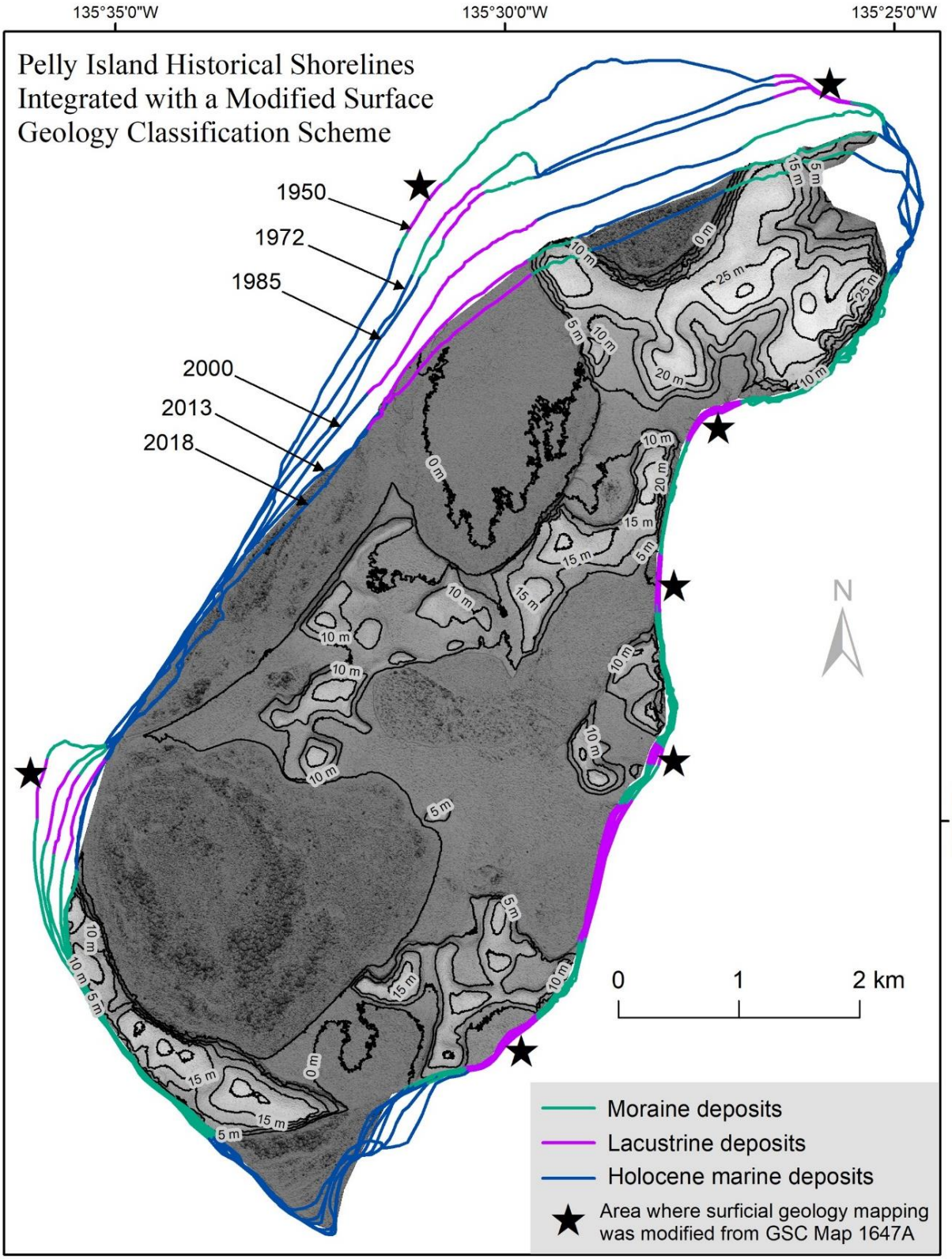

Figure 3.7: Pelly Island historical shorelines integrated with our modified surface geology classification scheme. Background is hillshaded DEM with 5m contour lines courtesy of Porter et al., 2018, "ArcticDEM".

Chapter 4: Results

4.1 Volumetric Analysis

4.1.1 Digital Surface Model Accuracy Validation

The point-to-raster validations of the DSMs reveal $RMSE_Z$ values ranged from 0.005m – 0.071m (Table 3). Standard deviation (SD) had a range between 0.005m – 0.059m. For the 2017 DSM with no associated validation data, all values for the SD and $RMSE_Z$ are replaced by three times the ground sample distance (GSD) (0.12 m for 2017) and are indicated as an "X" in Table 3 (pix4d.com, 2020).

Table 3: Accuracy validation for each DSM. For each flight the number of ground control points (GCPs), independent check points (n), the mean, standard deviation (SD), root mean squared error of the vertical component (RMSEz).

Date	GCPs (#)	n	Mean (m)	SD (m)	$RMSE_Z$ (m)
August 2016	17	3	-0.001	0.005	0.005
August 2017	5	1	0.091	X	X
August 2018	13	4	-0.040	0.058	0.071
August 2019	12	7	-0.003	0.059	0.060

4.1.2 Volumetric Change

A volumetric analysis was conducted for a 450 m stretch of shoreline on the rapidly eroding NW cliffs of Pelly Island (Figure 4.1) for the 2016 to 2019 observation period to determine the volume of sediment delivered to the nearshore. The total volume change for the entire observation period of 2016 to 2019 was 506 230 m^3 with a Level of Detection (LoD) threshold of 0.39 m^3 (99.5 % confidence interval) (Table 4). The total volume change for the 2016 to 2017 period was 184 487 m^3 with a LoD threshold of 0.48 m (99.5% confidence interval) and represented 36% of

the total volume change from 2016 to 2019. The total volume change for the 2017 to 2018 period was 152 864 m³ with a LoD threshold of 0.45 m (99.5% confidence interval) and represented 30% of the total volume change from 2016 to 2019. The total volume change for the 2018 to 2019 period was 168 083 m³ with a LoD threshold of 0.31 m (95% confidence interval) and represented 33% of the total volume change from 2016 to 2019. When normalizing the volume change rates for each meter of shoreline (length of shoreline was 450 m), the 2016 to 2017 period eroded at 410 m³ per meter, the 2017 to 2018 period eroded at 339 m³ per meter, the 2018 to 2019 period eroded at 373 m³ per meter. The entire observation period from 2016 to 2019 eroded at an average annual rate of 375 m³ per meter. Using the estimate for ground ice volume of 54% calculated by Dallimore et al. (1996) for similar morainal deposits on Richards Island adjacent to Pelly Island, we determined that the estimated volume of sediment delivered to the nearshore from the 2016 to 2017 period was 84 864 m³, from the 2017 to 2018 period was 70 317 m³, from the 2018 to 2019 period was 77 318 m³, and for the entire observation period from 2016 to 2019 was 232 865 m³ (Table 4).

Table 4:Results of the volumetric change analysis using 99.5% confidence interval to determine the Level of Detection for each observation period.

State	Year	Level of Detection Treshold (m)	Total Volume Change (m³)	Ground Ice Volume Estimate (54%) (m³)	Sediment Volume Estimate (m³)
Eroding	2016 to 2017	0.48	184 487	99 623	84 864
Eroding	2017 to 2018	0.45	152 864	82 546	70 317
Eroding	2018 to 2019	0.31	168 083	92 765	77 318
Eroding	2016 to 2019	0.39	506 230	273 364	232 865

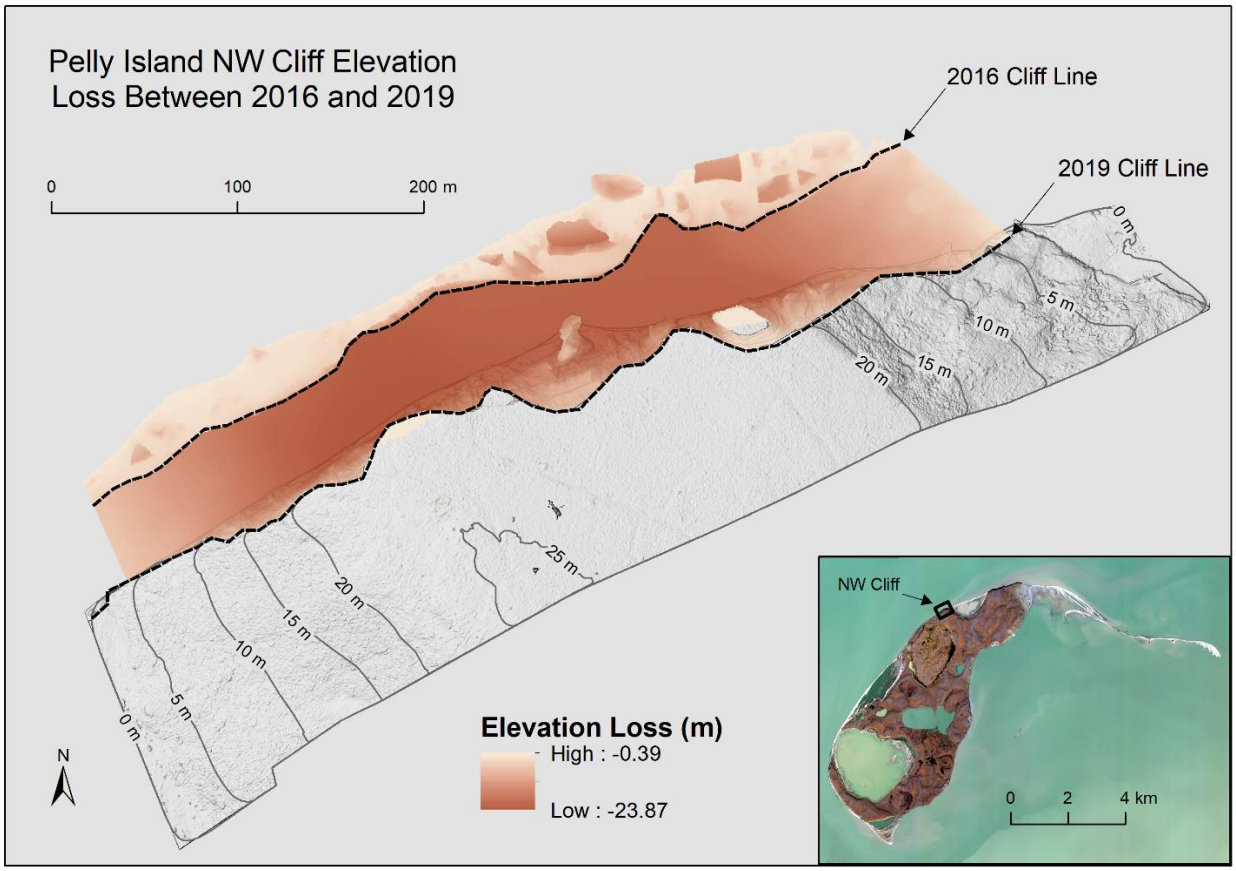

Figure 4.1: A DSM of difference showing the elevation loss on the NW cliff of Pelly Island from 2016 to 2019 with a hillshaded 2019 DSM with 5m contours as a background. The 2016 and 2019 cliff line are represented by dashed lines.

4.2 Spatial and Temporal Variability of Shoreline Change Rates

The linear regression shoreline change rate during the 1950-2018 observation period was -3.8 $m \cdot a^{-1}$, with 377 of 550 transects having a p value less than or equal to 0.05, therefore suggesting significant differences in rates of retreat between years. In comparison, the mean EPR for Pelly Island from 1950 to 2018 was -4.5 ± 0.9 $m \cdot a^{-1}$ (Table 5), with 88% percent of the shoreline retreating and 12% prograding (Figure 4.2). The mean EPR initially decreased from -3.4 ± 0.5 $m \cdot a^{-1}$ in the 1950-1972 period, to -2.2 ± 0.7 $m \cdot a^{-1}$ in the 1972-1985 period. This was followed by an increase in retreat, with a mean EPR of -4.4 ± 0.6 $m \cdot a^{-1}$ in the 1985-2000 period, and -5.5 ± 0.7

$m \cdot a^{-1}$ in the 2000-2018 period. The mean EPR from the 2000-2013 period was -4.6 ± 0.53 $m \cdot a^{-1}$, which was followed by a marked increase in retreat rates, with mean EPR rates of -8.0 ± 2.1 $m \cdot a^{-1}$ for the 2013-2018 period. The 2013-2018 observation period also showed the greatest variability in EPR with a standard deviation of 11.1 $m \cdot a^{-1}$ (Table 5).

Table 5: EPR Statistics for Pelly Island. The error associated with mean EPR is ± 0.9 $m \cdot a^{-1}$, which is the mean dissolution of accuracy (DOA) for all years.

Observation period	**Mean EPR ($m \cdot a^{-1}$)**	**Standard Deviation ($m \cdot a^{-1}$)**	**Significant Erosion (-2 Σ) ($m \cdot a^{-1}$)**	**Significant Progradation (+2 Σ) ($m \cdot a^{-1}$)**
1950-1972	-3.4 ± 0.9 $m \cdot a^{-1}$	6.6	-16.6	9.8
1972-1985	-2.2 ± 0.9 $m \cdot a^{-1}$	3.7	-9.7	5.2
1985-2000	-4.4 ± 0.9 $m \cdot a^{-1}$	8.3	-21.0	12.1
2000-2013	-4.6 ± 0.9 $m \cdot a^{-1}$	6.9	-18.3	9.2
2013-2018	-8.0 ± 0.9 $m \cdot a^{-1}$	11.1	-30.3	14.3
1950-2018	-4.5 ± 0.9 $m \cdot a^{-1}$	8.0	-20.4	11.4

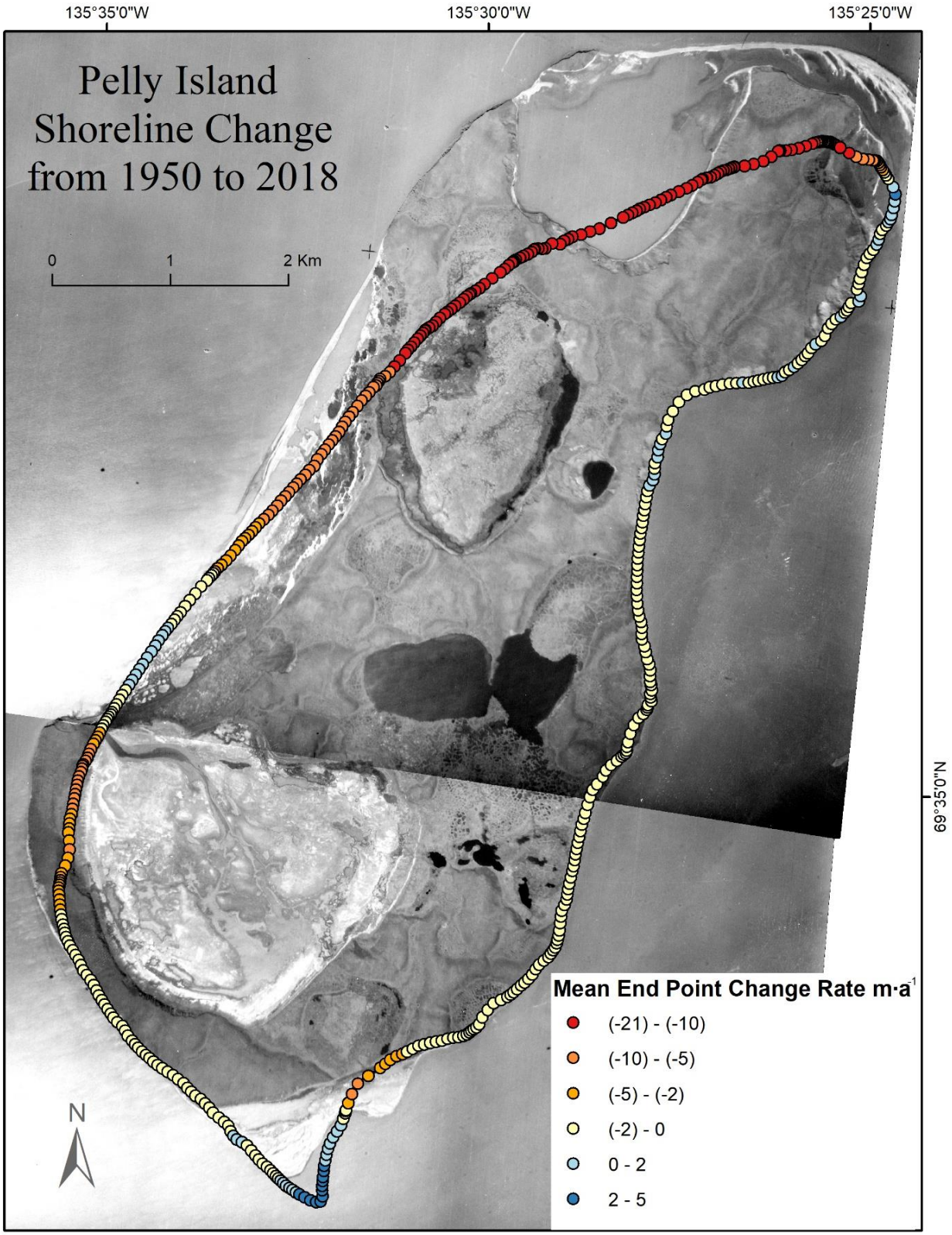

Figure 4.2. The Mean End Point Rate from 1950 to 2018 superimposed on Pelly Island's 2018 digitized shoreline with a 1950 image of Pelly Island as a background.

Of the 550 shoreline change transects, 293 were in the Northwestern (NW) zone and 257 were in the Southeastern (SE) Zone (Figure 3.5). In the NW zone 96% of the transects had shoreline change rates which were retreating and 4% were prograding, while 80% of SE Zone transects had shoreline change rates which were retreating and 20% prograding. The mean retreat rate for all transects in the NW zone was 8.3 ± 0.9 $m \cdot a^{-1}$ in the 1950-2018 observation period, in comparison the mean retreat rate for all transects in the SE zone was 0.4 ± 0.9 $m \cdot a^{-1}$ (Table 6). The NW zone showed the greatest variation in EPR with a standard deviation of 5.4 $m \cdot a^{-1}$ compared to 1.3 $m \cdot a^{-1}$ in the SE zone of the island. The transects in the NW zone of Pelly Island experienced the highest retreat rates with values up to -21 ± 0.9 $m \cdot a^{-1}$ and progradation rates up to 0.6 ± 0.9 $m \cdot a^{-1}$ (see *Pelly_Supertable.xls* in supplementary information database). In the SE zone, mean EPR rates were less negative and ranged from -5.7 ± 0.9 $m \cdot a^{-1}$ to 4.4 ± 0.9 $m \cdot a^{-1}$. The SE zone had positive mean EPR rates (indicating progradation) greater then the DOA (0.9 $m \cdot a^{-1}$) whereas the NW zone did not.

Table 6: EPR Statistics generalized for NW and SE side from 1950 to 2018. The error associated with mean EPR is the mean of the DOA errors for all years.

Spatial and Temporal Analysis	**NW Zone**	**SE Zone**
Number of transects	293	257
Mean EPR ($m \cdot a^{-1}$)	-8.30 ± 0.9 $m \cdot a^{-1}$	-0.4 ± 0.9 $m \cdot a^{-1}$
Standard deviation ($m \cdot a^{-1}$)	5.4	1.3
Significant erosion (-2 Sigma) ($m \cdot a^{-1}$)	-19.0	-3.0
Significant progradation (+2 Sigma) ($m \cdot a^{-1}$)	2.5	2.0

The mean EPR was also calculated for the three surficial geology classes for each observation period. During the 1950-2018 period lacustrine deposits accounted for an average of 17% of the total transects for each historical shoreline in the study, the morainal deposits accounted for a mean of 37%, and the Holocene marine deposits accounted for a mean of 38% of the transects. Although lower in coverage, the lacustrine deposits had the highest mean EPR (Figure 6) in all

observation periods except for the 1950-1972 observation period, when Holocene marine deposits had the greatest mean EPR. The Holocene marine deposits were the most represented class in terms of percentages of transects in each observation period prior to 2000, and the morainal deposits were most represented in the 2000-2013 and 2013-2018 periods. An increase in retreat for all three surficial geology classes occurred during the 2000-2013 period, and the 2013-2018 period (Table 7).

Table 7: Mean EPR rates for each surface geology class for the entire island, NW zone, and SE zone. Percentage of mean transects represented by surface geology class also included.

Surficial geology	EPR entire island 1950-2018 (± 0.9 m·a^{-1})	EPR NW zone 1950-2018 (± 0.9 m·a^{-1})	EPR SE zone 1950-2018 (± 0.9 m·a^{-1})	Mean Transects (%)
Lacustrine	-5.3	-12.0	-0.8	17
Moraine	-2.7	-5.7	-0.4	37
Holocene	-5.0	-7.3	-0.9	38

Due to the mobile nature of modern beach deposits and their natural ability to rebuild and readjust themselves (lacustrine deposits and the moraine deposits do not share this dynamic equilibrium), a separate analysis on the control of differing surficial geology on shoreline change in the NW and SE zone was conducted, excluding the Holocene beach deposit class. When isolating the NW zone of Pelly Island, the lacustrine deposits hosted the highest retreat rates in each of the observation periods (Figure 6). Only in the SE zone of Pelly Island, during the 1950-1972 observation period, did the moraine deposits have slightly higher mean EPR compared to the lacustrine deposits. However, the mean EPR values for the SE zone of Pelly Island were not found to be most negative and were generally within the DOA range. During the 1972-1985 period the moraine deposits had a positive mean EPR indicating progradation, this is due to the SE zone of Pelly Island having a prograding cuspate foreland and active thermokarst slumps with mud lobes which prograded into the ocean.

Manson and Solomon's (2007) storm count for the 1958-2000 period indicate that storms may have been a control on coastal erosion rates for Pelly Island during the 1972 to 1985 period. The decreased mean erosion rates observed in the 1972 to 1985 period, when compared to the 1950-1972 and 1985-2000 periods, did correlate with a lower number of storms (and associated lower wave energy) in the 1972-1985 period (Table 8, Figure 4.3). The higher erosion rates observed on Pelly Island during the 1950-1972 period (-3.4 ± 0.9 m·a^{-1}), and the 1985-2000 period (4.4 ± 0.9 m·a^{-1}) could be related to stormy periods on Pelly Island during the early 1960s, and late 1980s to early 1990s identified by Manson and Solomon (2007). The most storms (n=36) occurred in the 1950-1972 period (Table 8).

Table 8: Storm count and mean EPR for each observation period are tabulated. Record of storms from 1950 to 2000 were sourced from Manson and Solomon (2007).

Observation Period	Number of wind events exceeding 50 km h^{-1}	Mean EPR (m·a^{-1})	Storms/yr
1950-1972	36	-3.4 ± 0.5	1.64
1972-1985	23	-2.2 ± 0.7	1.77
1985-2000	30	-4.4 ± 0.6	2.00
2000-2013	3	-4.6 ± 0.5	0.23
2013-2018	5	-8 ± 2.1	1.00

Based on the 2005 to 2018 Pelly Island wind data, storm events could have had less influence on coastal erosion since 2000. From 2005 to 2013 there were only three storms recorded, which was a very notable drop in storm count compared to the storm count for observation periods from 1958 to 2000 compiled by Manson and Solomon (2007). However, erosion rates in the 2000-2013 period were comparable to those for the 1985-2000 and 1950-1972 periods (Table 5). During the 2013-2018 period there were only five storms recorded, which is another noteworthy drop in storm count compared to the 1958-2000 period and does not correlate with the observed increase in erosion during this period. This indicates that another factor could be driving the high rates of erosion, or that there are errors in the historical wind speeds and directions obtained for Pelly Island during the 2005 to 2018 period (Table 8).

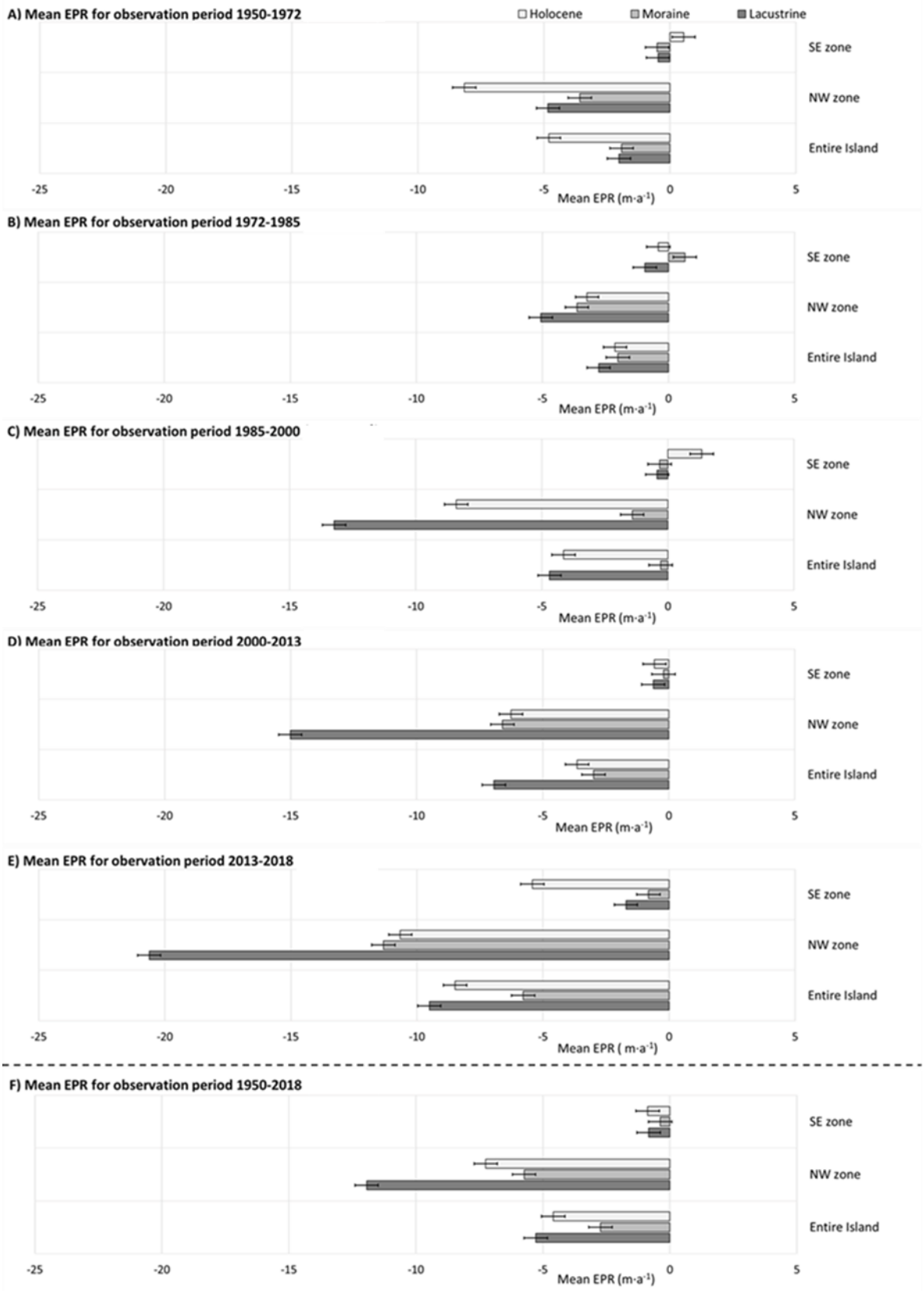

Figure 4.3. The Mean End Point Rate for the Northwest (NW) zone, Southeast (SE) zone and entire island for each surface geology class.

Chapter 5: Discussion and Conclusion

Our research quantified shoreline change rates and investigated the influence of surficial geology and exposure to storms on shoreline change dynamics for Pelly Island between 1950 and 2018.

5.1 Rates of Coastal Retreat of Unconsolidated Permafrost Coast are increasing

The average annual LRR rate for Pelly Island during the 1950-2018 observation period was -3.8 $m \cdot a^{-1}$, with 377 of 550 transects having a p value equal to or below 0.05 and an average standard error of the coefficient of the linear regression of 0.6 $m \cdot a^{-1}$. This would indicate that 68% of the shoreline change rates changed significantly between 1950 and 2018, and the shoreline change rate is most likely to change by 0.6 $m \cdot a^{-1}$. In order to better understand the shoreline change rates for each observation period, the EPR was calculated for all observation periods (Table 5).

When comparing the decadal shoreline change rates (excluding the 2013 historical shoreline), the mean EPR rates increased in retreat by 1m in three of the four observation periods (-3.4 ± 0.5 in the 1950-1972 period, -4.4 ± 0.6 $m \cdot a^{-1}$ in the 1985-2000 period, -5.5 ± 0.7 $m \cdot a^{-1}$ in the 2000-2018 period). During the 1950-1972 period, the retreat rate decreased from -3.4 ± 0.5 to -2.2 ± 0.7, which be related to decreased number of storms in the region during this time (Solomon and Manson 2007). Increased in shoreline retreat rates since the early 2000s has also been reported in other shoreline change studies in the circum-Arctic (Nielsen et al, 2022 Jones et al, 2020). Our data agrees with Solomon (2005) that Pelly Island has historically had the highest retreat rates in the Canadian Beaufort Sea up to the year 2000, and when comparing our reported change rates for the 2000-2018 period (-5.5 ± 0.7 $m \cdot a^{-1}$) with other shoreline change reports in the Canadian

Beaufort Sea since 2000 (e.g Irrgang et al, 2018; Obu et al, 2016; Lim et al, 2020; Berry et al, 2021; O'Rourke 2017) our data suggest that Pelly continues to be the location with the highest reported shoreline change rates in the Canadian Beaufort Sea.

When including the 2013 historical shoreline in the comparison of mean EPR rates (no longer decadal shoreline change rates), the mean EPR rate during the 2013 to 2018 observation period were the most negative (-8.0 ± 2.1 $m \cdot a^{-1}$), almost twice as negative as the mean EPR for the 2000 to 2013 observation period (Table 5). This is likely due to the comparison of a decadal shoreline change rate from the 2000-2013 period with an observation period which is half its length in time, since decadal shoreline change rates are less influenced by short-term non-linear nature of shoreline change rates. This is exemplified by the mean EPR for the 2000-2018 period, which was -5.5 ± 0.7 $m \cdot a^{-1}$ in the 2000-2018 period. However, the inclusion of the 2013 historical shoreline (derived from the image used for co-registration of all other imagery) still adds value to our investigation of shoreline change rates on Pelly Island. It is important to note that a mean EPR of -46.7 ± 2.1 $m \cdot a^{-1}$ was calculated for a transect in the NW zone of Pelly Island during the 2013 to 2018 period. This shoreline change rate was calculated for a transect located along a section of shoreline classified as moraine deposits, and the adjacent transects had similarly high rates of shoreline retreat. When comparing this this extreme retreat rate with other more local change rates for similarly smaller sections of shoreline (e.g.: Lim et al, 2020; Berry et al, 2021; O'Rourke 2017; Irrgang et al, 2018; Obu et al, 2016) could be the greatest local retreat rate reported in the Canadian Beaufort Sea, and possibly the circum-Arctic.

The compilation of storms (with mean speeds > 50 $km \cdot h^{-1}$, duration > 6 hours, wind vector cut off to only include 270° to 360° direction) during the open-water season (June to October) for each observation period was aggregated to identify relationships between storm count and mean

shoreline change rates on Pelly Island (Table 8, Figure 3.6). Storms were found to be a control on coastal erosion from 1950 to 2000. During the 2000 to 2013 observation period (which had missing data from 2000 to 2005), there was a marked decrease in storms with only three storms recorded at the Pelly Island weather station compared to 30 storms calculated by Manson and Solomon (2007) for the 1985-2000 observation period (Table 8). Despite this, both observation periods had similar erosion rates regardless of the number of storms. The 2013 to 2018 period also had very low number of storms compared to the number of storms calculated by Manson and Solomon (2007) during the 1950-2000 period, with only five storms recorded during a period where mean erosion rates had almost doubled all other observation periods (Table 8). The decreased number of storms in the last two decades could be due to the two different methods for compiling wind data, with our storm count from 2005 to 2018 derived from the Pelly Island weather station, whereas the 1958 to 2000 storm count used in our project was derived from Manson and Solomon (2007) which combined wind data from weather stations from Tuktoyaktuk from 1958 to 2000 with wind data from the Pelly Island wind station from 1994 to 2000 to create a synthetic storm count for Pelly Island from 1958 to 2000. It is worth noting that wind conditions on Pelly Island are known to be more characteristic of marine winds (Manson and Solomon 2007), having much greater speeds and variability when compared to the other more sheltered or inland wind stations, such as the Tuktoyaktuk wind stations used in the synthetic storm record created by Manson and Solomon (2007). Therefore, we would expect greater number of storms to be recorded when using data strictly derived from the Pelly Island weather station compared to the synthetic storm record which includes wind data from Tuktoyaktuk weather stations. O'Rourke (2017) compiled storms for the Beaufort Mackenzie region from 2008 to 2015 using wind data from a Tuktoyaktuk weather station and yielded storm count results comparable to those found by Manson and Solomon (2007) in the

1958-2000 period, however O'Rourke (2017) used a storm criteria which only identified storms over 50 $km \cdot h^{-1}$, with no reported criteria on storm duration or storm direction (wind vector cut off), which would likely yield higher storm counts compared to the storm count criteria used in our study and in the Manson and Solomon (2007) study. It is possible that the decreased storm count from 2005 to 2018 in our study is accurate (although seems unlikely), which would be in line with the prediction from Manson and Solomon (2007) that storms in the Beaufort were going to decrease in frequency and increase in strength as we approach 2050. When normalizing storms it was found that the number of storms has only decreased slightly post 2000s. Additional studies on storms are recommended to confirm if there has been a decrease in storms using the storm definition set out by Manson and Solomon (2007), and further analysis of storms without a wind vector cut off would be useful to determine the influence of storms form the south-east.

5.2 Shoreline change rates are controlled spatially by coastal exposure and local geology

The NW zone of Pelly Island (Figure 3.5), which faces the predominant storm direction to the Northwest (Lintern et al., 2013; Solomon 2005), had a mean EPR of -8.27 ± 0.9 $m \cdot a^{-1}$ during the 1950 to 2018 observation period, in stark comparison the more sheltered SE zone had a mean EPR of -0.44 ± 0.9 $m \cdot a^{-1}$ (Table 6). During the 1950 to 2018 observation period, the NW zone had 96% of its transects retreating and 4% prograding and the SE zone had 80% of it transects retreating and 20% prograding. This major difference in coastal retreat rates is due to the exposure of the NW zone to the predominant storm direction, allowing wind driven waves and associated high water level during storm surges to erode the coastline. However, both the NW zone and SE zone of Pelly Island have been primarily retreating and not prograding. The NW zone experienced

the most shoreline retreat, having eroded by as much as 1.4 km over the 1950 to 2018 period (see supplemental information database *Pelly_Supertable.xls*). The Canadian Beaufort Sea is known to be quite shallow (Lintern et al., 2013). Subtle variations in nearshore bathymetry could also play a role in the higher retreat rates observed in the NW zone of Pelly Island since it has a deeper nearshore profile compared to the SE zone possibly allowing larger waves to reach the shoreline (see bathymetric contours in Figure 1.1).

The ice-rich moraine deposits (and underlying units) on Pelly Island are found in higher elevation headlands (5 to 30 m) compared to the ice-rich lacustrine deposits which occupy lower lying headlands. Although lower in coverage (represented an average of %16 of the transects for each historical shoreline), lacustrine deposits had the most negative change rates for all but one other observation period. When excluding the Holocene marine deposits from our analysis and only comparing the different change rates for lacustrine and moraine deposits in the NW and SE zone of Pelly Island, lacustrine deposits had the highest coastal retreat in all observation periods except for the SE zone during the 1950 to 1972 observation period. It is important to note that the portion of moraine deposits in the south-eastern portion of the NW zone may be contributing to the reduced retreat rates for moraine deposits in the NW zone because a high percentage of the NW moraine class transects are along this non-eroding (drift-aligned) coast, parallel to the dominant direction of wave approach. The implementation of a surficial geology classification scheme combined with our mean shoreline change rates agrees with other studies (Solomon 2005, Pelletier and Medioli 2014) that the lower lying ice-rich lacustrine deposits are more susceptible to coastal retreat.

Coastal change in the Beaufort Sea is driven by the impact of periodic storms and long-term rising sea level (Manson and Solomon 2007; Lintern et. al. 2013; Solomon 2005; Berry et.

al. 2021; Scharffenberg et. al. 2019; Kim et. al. 2021). It has been suggested that local geological and morphological conditions could influence coastal change in the Beaufort Mackenzie region (Solomon 2005). Lacustrine deposits are absent on the other two islands in the outer island zone identified by Solomon (2005), which could help explain why Pelly Island has such high coastal retreat rates in comparison (Lim et al, 2020), the increased retreat rates observed from lacustrine deposits on Pelly Island.

Previous research on the historical (1972 to 2000) shoreline change rates in the Canadian Beaufort Mackenzie region was conducted by Solomon (2005), who reported the mean shoreline change rate for five zones, one of which was designated for the outer islands of the Mackenzie Delta and included Pelly Island (although shoreline change rates for Pelly Island specifically was not reported). Through Natural Resources Canada (NRCan) it was possible to access the data and results specifically for Pelly Island (including georeferenced historical imagery) from the Solomon (2005), allowing a direct comparison to the shoreline change rates for Pelly Island. A total of 136 transects were used in the Solomon (2005) study to calculate shoreline change rates. In comparison, our study used a total of 550 transects to calculate shoreline change rates.

First, we compared the two differently georeferenced historical imagery (1972, 1985, 2000) from our study, which was the same imagery used in the Solomon (2005) study, but co-registered to a high resolution satellite image of Pelly Island (2013 Geoeye). It was found that the position of the Southwestern shoreline of Pelly Island deviated by as much as 40 m for the 1972 and 1985 imagery used in the Solomon (2005) study, which is due to the Solomon (2005) study having used two images with very clear warping of one of two images in the 1972 period (southern image of Pelly), and one of two images in the 1985 period (southern image of Pelly again) due to georectification errors. Shoreline positions in all other areas of the Pelly Island imagery from the

1972 to 2000 Solomon (2005) study did generally agree with our 1972 to 2000 imagery which was co-registered (within 10m).

Shoreline change rates from 1972 to 2000 for our study and the Solomon (2005) study are found in Table 9. Our study calculated the mean shoreline change rate from 1972 to 2000 was -3.4 ± 0.7 $m \cdot a^{-1}$, whereas a mean shoreline change rate of -1.4 $m \cdot a^{-1}$ was found when analysing data from the Solomon (2005) study. Pelly Island was identified as having the highest retreat rate in the Beaufort-Mackenzie region from 1972 to 2000 in the Solomon (2005) study, with up to 22.5 $m \cdot a^{-1}$ ± 1 $m \cdot a^{-1}$of coastal retreat observed in the 1985 to 2000 period (the only shoreline change rate given for Pelly Island specifically). In comparison, our study found that Pelly Island had an even greater maximum retreat rate, with -26.7 ± 0.6 $m \cdot a^{-1}$ during the 1985 to 2000 period. When analysing the shoreline change data used in the Solomon (2005) study, we found that the maximum shoreline retreat distance calculated for Pelly Island was -429.2m, in contrast our study found that Pelly Island had a maximum shoreline retreat of -554.6 m (Table 9). Two reasons for the differences in shoreline change rates compared to those in the Solomon (2005) study are primarily due to our project having almost double the transects used in the shoreline change analysis, which could lead to better representation of shoreline change rates. A second reason is that our study had more accurate shoreline positions in the southern part of Pelly Island for the 1972 and 1985 period, due to two images used in the Solomon (2005) study which had shoreline position errors due to clear georectification errors in one of two images used in 1972, and one of two images used in 1985.

Table 9: A comparison of the shoreline change results in our study using AMBUR (Jackson 2009) compared to the shoreline change results in Solomon (2005) using DSAS (Thieler, 2009).

EPR 1972-2000	Solomon (2005), using DSAS	Our study using AMBUR
Mean shoreline change rate	-1.4 $m \cdot a^{-1}$	-3.4 ± 0.9 $m \cdot a^{-1}$
Maximum progradation per year	3.8 $m \cdot a^{-1}$	6.8 ± 0.9 $m \cdot a^{-1}$
Maximum erosion per year	-15.3 $m \cdot a^{-1}$	-19.8 ± 0.9 $m \cdot a^{-1}$
Maximum progradation distance	107.5 m	190.3 m
Maximum retreat distance	-429.2 m	-554.6 m
Transect Count	136.0	550.0

To better highlight differences in these two methods, we compared shoreline change results from five adjacent transects from the northwestern zone for each study (Table 10). The chosen location for comparison was on the Northwestern zone of Pelly Island, an area where georectification and shoreline position generally agreed for both studies compared to other areas. Four out of five transects (all adjacent to each other) compared were found to have marked differences for rates of coastal retreat (Transects A to D). However, there was an instance where the transect in each study agreed almost perfectly (Transect E), indicating that both methods could produce very similar results. The differences in shoreline change rates and shoreline retreat is thought to be due to differences in the greater number of transects used in our study and the two images with georectification errors used in the Solomon (2005) study.

Table 10: A comparison of transect results from this research to Solomon (2005) results along the NW cliff of Pelly Island

Transects from NW of Pelly 1972 to 2000	Solomon (2005), using DSAS		Our study, using AMBUR	
	Retreat (m)	EPR ($m \cdot a^{-1}$)	Retreat (m)	EPR ($m \cdot a^{-1}$)
Transect A	-239.8	-8.6	-274.7	-9.8
Transect B	-229.7	-8.2	-288.6	-10.3
Transect C	-265.7	-9.5	-356.1	-12.7
Transect D	-349.7	-12.5	-410.4	-14.7
Transect E	-429.1	-15.3	-429.3	-15.3

The total volumetric erosion for the NW cliffs (Figure 4.1) of Pelly Island from 2016 to 2019 was 506 230 m^3 (with a 95 % confidence interval), of which an estimated 232 865 m^3 of sediment and nutrients were liberated into the nearshore. The 450 m stretch of the NW cliffs fluctuate in elevation from 1 m to 24 m, with approximately 1 m being moraine (minimal ice content), and the underlying units comprising the rest of the cliff (high ice content). When normalizing volumetric erosion, it was estimated that the 450 m stretch of coastline studied was eroding at 373 $m^3\ m^{-1}\ a^{-1}$. In comparison, Obu et al. (2016) estimated that the rate of volumetric erosion from block failures on the north side of Herschel Island (Yukon) was 73 $m^3\ m^{-1}\ a^{-1}$ between 2004 and 2013, and Berry et al. 2020 reported that the block failures on Pullen Island (NWT) have been eroding at 37.5 $m^3\ m^{-1}\ a^{-1}$ from 2016 to 2017. The presence of block-failures along coastal segments has been more closely correlated with environmental forcing as opposed to planimetric erosion rates (Obu et al., 2016), which could indicate that the higher rates of volumetric erosion observed along the NW cliffs of Pelly Island are due to greater exposure to environmental forcing and wave-action compared to Herschel Island. In contrast, Pullen Island is adjacent to Pelly Island (40km away) and shares similar coastal exposure to the predominant storm direction and has volumetric erosion rates for block-failures which are much lower than those at Herschel Island (130km NW of Pelly). Based on storm data by Berry et al (2020) for Pullen Island, the 2016 to 2017 period had storms of greater duration and intensity compared to the 2017 to 2018 period of their study and resulted in greater volumetric erosion of block failures from 2016 to 2017. A similar observation was made for Pelly Island, which had the highest volumetric erosion rates during the 2016 to 2017 period and would have been affected by the same increase in storm intensity and duration. Cliffs over 30 metres generally have large volumetric erosion rates even while eroding at low planimetric erosion rates (Obu et al., 2016). The cliffs with block failures on Pullen Island

are only 5 m in elevation, therefore it can be assumed that Pelly Island's larger cliffs are the reason for the greater erosion rates observed on the NW cliffs. This could indicate that the combination of high elevation cliffs and coastal exposure to storms is driving the abnormally high volumetric erosion rates observed on Pelly Island.

Land loss and the liberation of high sediment and nutrient loads into the nearshore from rapid erosion of permafrost coasts has a significant impact on coastal ecosystems and the food security of northern communities (Semiletov et al. 2016; Ford et al. 2015; Johnson et al. 2003; Mars and Houseknecht 2007). Large quantities of sediment and nutrient loads can be released by coastal erosion (Rachold et al. 2004) and to quantify the proportions of these materials volumetric erosion data are required. Historically Arctic coastal erosion studies were mostly based on linear shoreline movements (planimetric coastal erosion) and land loss observations, with only a small quantity of studies estimating volume losses (volumetric coastal erosion). Volumetric coastal erosion was poorly understood due to the limitations of traditional remote sensing methods and the absence of high resolution DEMs (Obu et al. 2016). Mass fluxes of sediments and nutrients were based on the combination of planimetric shoreline movement rates and average cliff heights (e.g., Jorgenson and Brown 2005; Gunther et al 2013) and assumed that shoreline retreat correlates with volumetric erosion. The scarcity of volumetric data significantly reduces the accuracy of estimates for sediment and nutrient fluxes (Obu et al. 2016). However, the recent advent of higher temporal and spatial resolution remote sensing methods (<1m satellite imagery, LiDAR, UAV-SfM) has improved the ability to capture short-term geomorphic change in the Arctic while using DEMs (Jones et al. 2013; Gunther et al. 2015; Obu et al. 2016; Jones et al. 2018; Cunliffe et al. 2019; Berry et al. 2021, Clark et al. 2020).

Chapter 6: Conclusions

By quantifying the shoreline change rate for the 1950-2018 observation period and comparing the influence of surficial geology and exposure to storms on shoreline change rates it was possible to draw the following conclusions about the coastal dynamics on Pelly Island.

- The average annual LRR rate for Pelly Island during the 1950-2018 observation period was -3.8 $m \cdot a^{-1}$, with 377 of 550 transects having a p value equal to or below 0.05.

- A mean EPR of -5.5 ± 0.7 $m \cdot a^{-1}$ was calculated for the 2000-2018 period, and a maximum retreat rate of 46.7 ± 2.1 $m \cdot a^{-1}$ was recorded during the 2013-2018 observation period.

- Shoreline exposure to the predominant storm direction from the Northwest was found to be a major influence on shoreline change rates in all observation periods, with the NW zone of Pelly Island (Figure 3.5), which faces the predominant storm direction to the Northwest, had a mean EPR of -8.27 ± 0.9 $m \cdot a^{-1}$ during the 1950 to 2018 observation period. In stark comparison the more sheltered SE zone had a mean EPR of -0.44 ± 0.9 $m \cdot a^{-1}$ (Table 6).

- The NW zone experienced the most shoreline retreat, having eroded by as much as 1.4 km over the 1950 to 2018 period.

- Although lower in coverage compared to moraine deposits and modern Holocene beach deposits (represented an average of 16% of the transects for each historical shoreline), greater retreat rates were observed for lacustrine deposits in all but one observation period.

- When normalizing volumetric erosion, it was estimated that the 450m stretch of the NW cliffs of Pelly Island coastline were eroding at 373 m^3 m^{-1} a^{-1} (± 0.39 m^3).
- Pelly Island continues to host the highest retreat rates in the Canadian Beaufort Sea, and our study reports that Pelly Island's retreat rates have been increasing since the year 2000.

Pelly Island continues to be an extreme example of shoreline retreat in the Mackenzie-Beaufort region. Further investigation is needed to define the direct impacts of environmental forcing (wind, waves, air temperatures) on the island and the implications this could have on coastal dynamic processes of extreme change that have been observed through this study.

Bibliography

Are, F.E.. (1988). Thermal abrasion of sea coast. Polar Geography and Geology 12, 1–157.

Adams, M.. (1807). Some account of a journey to the frozen sea, and of the discovery of the remains of a mammoth. Philosophical Magazine, 29, 141-143.

Atkinson, D.E.. (2005). Observed storminess patterns and trends in the circum-Arctic coastal regime. Geo-Marine Letters. doi: 10.1007/s00367-004-0191-0

Beaufort Sea Partnership Integrated Ocean Management Plan (IOMP) for the Beaufort Sea: 2009 and Beyond (2009). 'Integrated Ocean Managemental Plan for the Beaufort Sea: 2009 and beyond' [Online] Available from http://www.beaufortseapartnership.ca/wp-content/uploads/2015/04/Integrated-Ocean-Management-Plan-for-the-Beaufort-Sea.pdf [accessed: September 10th, 2020].

Berry, H., Whalen, D., Lim, M., (2021). 'Long-term ice-rich permafrost coast sensitivity to air temperatures and storm influence: lessons from Pullen Island, NWT', *Arctic Science*, 00, p1-23, dx.doi.org/10.1139/as-2020-0003

Berner, R. A. (1982). Burial of organic carbon and pyrite sulfur in the modern ocean: its geochemical and environmental significance. *Am. J. Sci.;(United States), 282*.

Brasington, J., Langham, J., & Rumsby, B. (2003). Methodological sensitivity of morphometric estimates of coarse fluvial sediment transport. *Geomorphology, 53*(3-4), 299-316.

Brown, J., Jorgenson, M.T., Smith, O.P., Lee, W.. (2003). Long-term rates of erosion and carbon input, Elson Lagoon, Barrow, Alaska. Proceedings of the 8th International Conference on Permafrost, 101–106.

Burn, C.R., Lewkowicz, A.G.. (1990). Retrogressive thaw slumps. The Canadian Geographer, 34, 273–276.

Carrivick, J. L., Smith, M. W., & Quincey, D. J. (2016). *Structure from Motion in the Geosciences.* John Wiley & Sons.

Couture, N. J., Irrgang, A., Pollard, W., Lantuit, H, & Fritz, M. (2018). 'Coastal erosion of permafrost soils along the Yukon Coastal Plain and fluxes of organic carbon to the Canadian Beaufort Sea', *Journal of Geophysical Research: Biogeosciences*, 123, p406-422. https://doi.org/10.1002/2017JG004166

Cunliffe, A.M., Tanski, G., Radosavljevic, B., Palmer, W.F., Sachs, T., Lantuit, H., et al. (2019). Rapid retreat of permafrost coastline observed with aerial drone photogrammetry. Cryosphere, 13: 1513–1528. doi: 10.5194/tc-13-1513- 2019.

Clark, A., Moorman, B., Whalen, D., Fraser, P., (2021). Arctic coastal erosion: UAV-SfM data collection strategies for planimetric and volumetric measurements. Arctic Science, 7: 605-633. Doi: dx.doi.org/10.1139/as-2020-0021

Davidson-Arnott, Robin & G.D, Robin. (2010). Davidson-Arnott, R.G.D., 2010. Introduction to Coastal Processes and Geomorphology. Cambridge University Press, Cambrige.

Dallimore, S.R., Wolfe, S.A., Solomon, S.M.. (1996). Influence of ground ice and permafrost on coastal evolution, Richards Island, Beaufort Sea coast, N.W.T. Can. J. Earth Sci. 33, 664-675.

de Krom, V.. (1990). Retrogressive thaw slumps and active layer slides on Herschel Island, Yukon. M.Sc. Thesis,McGill University, Montréal, Québec.

Eltner, A., Kaiser, A., Castillo, C., Rock, G., Neugirg, F., & Abellán, A. (2016). Image-based surface reconstruction in geomorphometry–merits, limits and developments. *Earth Surface Dynamics*, *4*(2), 359-389.

Forbes, D. L., Solomon, S. M., and Frobel, D. (1995). 'Report of the 1992 coastal surveys in the Beaufort Sea', *Geological Survey of Canada Open File*, 3053, 53. Doi:10.4095/203482.

Ford, J.D., McDowell, G., and Pearce, T. (2015). The adaptation challenge in the Arctic. Nat. Clim. Change, 5(12): 1046–1053. doi: 10.1038/nclimate2723

Forest, A., Sampei, M., Hattori, H., Makabe, R., Sasaki, H., Fukuchi, M., Wassmann, P., Fortier, L.. (2007). Particulate organic carbon fluxes on the slope of the Mackenzie Shelf (Beaufort Sea): physical and biological forcing on shelf-basin exchanges. J. Mar. Syst., 68, 39–54.

Foster, E. R., Savage, R. J. (1989). 'Methods of historical shoreline analysis', *Coastal Zone*, *89*, 4434–4448.

French, H.M., (2007). The Periglacial Environment, third edition. John Wiley and Sons, New York.

Grigoriev, M.N., Rachold, V.. (2003). The degradation of coastal permafrost and the organic carbon balance of the Laptev and East Siberian Seas. Proceedings of the 8th international conference on Permafrost, 21–25, 319–324.

Günther, F., Overduln, P.P., Baranskaya, A., T. Opel, Grlgorlev, M. N.. (2013). Observing Muostakh Island disappear: erosion of a ground-ice-rich coast in response to summer warming and sea ice reduction on the East Siberian shelf. The Cryosphere Discuss, 7, 4101-4176. doi: 10.5194/tcd-7-4101-2013

Günther, F., Overduin, P.P., Yakshina, I.A., Opel, T., Baranskaya, A.V., and Grigoriev, M.N. (2015). Observing Muostakh disappear: permafrost thaw subsidence and erosion of a ground-ice-rich island in response to arctic summer warming and sea ice reduction. Cryosphere, 9: 151–178. doi: 10.5194/tc-9-151-2015.

Haas, F., Hilger, L., Neugirg, F., Umstädter, K., Bretiung, C., Fischer, P., . . . Schmidt, J. (2016). Quantification and analysis of geomorphic processes on a recultivated iron ore mine on the Italian island of Elba using long-term ground-based lidar and photogrammetric SfM data by a UAV. *Natural Hazards and Earth System Sciences, 16*(5), 1269-1288.

Hapke, C. J., Reid, D. (2007). 'National assessment of shoreline change, part 4: Historical coastal cliff retreat along the California coast. U.S', *Geological Survey Open File*, 1133, 51. Retrieved from https://pubs.usgs.gov/of/2007/1133/

Harper JR, Reimer PD, Collins AD (1985) Beaufort Sea physical shore-zone analysis. Geological Survey of Canada. Open File, vol 1689, 105.

Hill, P. R., Mudie, P. J., Moran, K., & Blasco, S. M. (1985). A sea-level curve for the Canadian Beaufort Shelf. *Canadian Journal of Earth Sciences*, *22*(10), 1383-1393.

Hill, P.R., Nadeau, O.C., (1989). Storm-dominated transport under storm-combined flows, Canadian Beaufort Sea. J Coast Re, 17, 507-516

Hill, P. R., Blasco, S. M., Harper, J. R., & Fissel, D. B. (1991). Sedimentation on the Canadian Beaufort shelf. *Continental Shelf Research*, *11*(8-10), 821-842.

Hill, P. R., Lewis, C. P., Desmarais, S., Kauppaymuthoo, V., & Rais, H. (2001). The Mackenzie Delta: Sedimentary processes and facies of a high-latitude, fine-grained delta. *Sedimentology*, *48*(5), 1047-1078.

Hmiznikov, P.K. (1937). Erosion of the shores of the Laptev Sea. Northern Sea Route. Leningrad; 122-133.

Hoque, M. A., & Pollard, W. H. (2016). Stability of permafrost dominated coastal cliffs in the Arctic. *Polar Science*, *10*(1), 79-88.

Irrgang, A. M., Lantuit, H., Mason, G. K., Gunther, F., Grosse, G., Overduin, P. P. (2018). 'Variability in rates of coastal change along the Yukon coast, 1951 to 2015', *Journal of Geophysical Research*, 123, 779-800, https://doi.org/10.1002/2017JF004326.

Jackson, C. W. (2009). 'The Ambur project: Analyzing Moving Boundaries Using R', *Department of Geology & Geography Georgia Southern University*. [Online]. Available from http://ambur.r-forge.r-project.org/ [accessed on January 19th 2020].

James, T.S., Henton, J.A., Leonard, L.J., Darlington, A., Forbes, D.L., Craymer, M., (2014). 'Relative Sea-level Projections in Canada and the Adjacent Mainland United States', *Geological Survey of Canada Open File*, 7737, 72 p. doi10.4095/295574

Jorgenson, M.T., Macander, M., Jorgenson J.C., Ping, C., Harden, J.. (2003). Ground-ice and carbon characteristics of eroding coastal permafrost at Beaufort Lagoon, northern Alaska. Proceedings of the 8th International Conference on Permafrost, 21–25, 495–500.

Jorgenson, M.T., Brown, J.. (2005). Classification of the Alaskan Beaufort Sea coast and estimation of carbon and sediment inputs from coastal erosion. Geo-Marine Letters 25, 69-80.

Johannessen, O. M., L. Bengtsson, M.W. Miles, S.I., Kuzmina, V.A., Semenov, G.V. Aleekseev, A.P., Nagurnyi, V.F., Zakharov, L., Bobylev, L.H., Pettersson, K., Hasselmann and H.P., Cattle. (2002). 'Arctic climate change – observed and modelled temperature and sea ice variability', *Nansen Environmental and Remote Sensing Centre Technical Report*, 218, pp22.

Johnson, K., Solomon, S., Berry, D., and Graham, P. (2003). Erosion progression and adaptation strategy in a northern coastal community. EBA Engineering Consultants Ltd

Jones, B.M., Hinkel, K.M., Arp, C.D., Eisner, W.R.. (2008). Modern erosion rates and loss of coastal features and sites, Beaufort Sea coastline, Alaska. Arctic, 61, 361-372.

Jones, B.M., Stoker, J.M., Gibbs, A.E., Grosse, G., Romanovsky, V.E., Douglas, T.A., et al. (2013). Quantifying landscape change in an arctic coastal lowland using repeat airborne LiDAR. Environmental Research Letters. 8(4): 045025. doi: 10.1088/1748- 9326/8/4/045025.

Jones, B.M., Farquharson, L.M., Baughman, C.A., Buzard, R.M., Arp, C.D., Grosse, G., et al. (2018). A decade of remotely sensed observations highlight complex processes linked to coastal permafrost bluff erosion in the Arctic. Environmental Research Letters. 13(11): 115001. doi: 10.1088/1748-9326/aae471.

Jones, B. M., Irrgang, A. M., Farquharson, L. M., Lantuit, H., Whalen, D., Ogorodov, S., Grigoriev, M., Tweedie, C., Gibbs, A. E., Strzelecki, M. C., Baranskaya, A., Belova, N., Sinitsyn, A., Kroon, A., Maslakov, A., Vieira, G., Groose, G., Overduin, P., Nitze, I., Maio, C., Overbeck, J., Bendixen, M., Zagórski, P., Romanovsky, V. E., (2020) 'Coastal permafrost erosion', *National Oceanic and Atmospheric Administration*, Administrative Report, noaa:27897, https://doi.org/10.25923/e47w-dw52 KW

Khon, V. C., Mokhov, I. I., Pogarskiy, F. A., Babanin, A., Dethloff, K., Rinke, A., Matthe, H., (2014). 'Wave heights in the 21st century Arctic Ocean simulated with regional climate model' *Geophysical Research Letters*, 41 (8), p2956-2961

Kim, J., Murphy, E., Nistor, I., Ferguson, S. and Provan, M., (2021). 'Numerical Analysis of Storm Surges on Canada's Western Arctic Coastline', *Journal of Marine Science and Engineering*, *9*(3), p.326.

Konopczak, A.M., Manson, G.K., and Couture, N.J. (2014). 'Variability of coastal change along the western Yukon coast'. *Geological Survey of Canada,* Open File Report, 7516. 81 pp. doi: 10.4095/293788.

Lane, S. N., Westaway, R. M., & Murray-Hicks, D. (2003). Estimation of erosion and deposition volumes in a large, gravel-bed, braided river using synoptic remote sensing. *Earth Surface Processes and Landforms: The Journal of the British Geomorphological Research Group, 28*(3), 249-271.

Lantuit H., Pollard, W.H.. (2005). Temporal stereophotogrammetric analysis of retrogressive thaw slumps on Herschel Island, Yukon Territory. Natural Hazards and Earth System Science, 5, 413-423.

Lantuit, H., Pollard, W.H.. (2008). Fifty years of coastal erosion and retrogressive thaw slump activity on Herschel Island, southern Beaufort Sea, Yukon Territory, Canada. Geomorphology 95, 84-102. Retrieved from http://www.sciencedirect.com/science/article/pii/S0169555X07001705

Lantuit, H., Atkinson, D., Overduin, P.P., Grigoriev, M., Rachold, V., Grosse, G., Hubberten, H.W.. (2011). Coastal erosion dynamics on the permafrost-dominated Bykovsky Peninsula, north Siberia, 1951-2006. Polar Research 30: 7341–7361.

Lantuit, H., Overduin, P.P, Couture, N., Wetterich, S., Aré, F., Atkinson, D., Borwn, J., Cherkashov, G., Drozdov, D., Forbes, D. L., Graves-Gaylord, A., Grigoriev, M., Hubberten, H., Jordan, J., Jorgenson, T., Ødegård, R. S., Ogorodov, S., Pollard, W. H., Rachold, V., Sedenko, S., Solomon, S., Steenhuisen, F., Streletskaya, I., Vasiliev, A. (2012). 'The Arctic Coastal Dynamics Database: A new classification scheme and statistics on Arctic permafrost coastlines', *Estuaries and Coasts*, 35 (2), p383-400. Doi:10.1007/s12237-010-9362-6.

Lantuit, H., Overduin, P.P., Wetterich, S.. (2013). Recent progess regarding permafrost coasts. Permafrost and Periglacial Processes, 24, 120-130. doi: 10.1002/ppp.1777

Lewkowicz, A.G.. (1987). Headwall retreat of ground-ice failures, Banks Island, North–west Territories. Canadian Journal of Earth Sciences, 24, 1077–1085.

Leffingwell, E.K.. (1919). The Canning River region, northern Alaska. US Geological Survey Professional Paper 109, 251pp.

Lewkowicz, A.G.. (1990). Morphology, Frequency and Magnitude of Active Layer Detachment Slides, Fosheim Peninsula, Ellesmere Island, N.W.T. Proceedings of the 5th Canadian Permafrost Conference. Université Laval, Quebec City, 111–118.

Lim, M., Whalen, D., J., Mann, P., Fraser, P., Berry, HB., Irish, C., Cockney, K., and Woodward, J., (2020) 'Effective monitoring of permafrost coast erosion: wide-scale storm impacts on outer islands in the Mackenzie Delta area', *Front. Earth Sci*. 8, 561322. Doi:10.3389/feart.2020.561322

Lintern, D.G., Macdonald, R.W., Solomon, S.M., Jakes, H.. (2013). Beaufort Sea storm and resuspension modeling. Journal of Marine Systems, 127, 14-25. doi: 10.1016/j.jmarsys.2011.11.015

Lavoie, D., Denman, K. L., & Macdonald, R. W. (2010). Effects of future climate change on primary productivity and export fluxes in the Beaufort Sea. *Journal of Geophysical Research: Oceans*, *115*(C4).

Fifty years (1935-1985) of coastal retreat west of Tuktoyaktuk, District of Mackenzie. Geological Survey of Canada, Paper 86-1A, 727-735.

Mackay, J.R.. (1963). Notes on the shoreline recession along the coast of the Yukon Territory. Arctic, 16, 103-116.

Mackay J.R.. (1972). Offshore permafrost and ground ice, southern Beaufort Sea. Canadian Journal of Earth Science 9, 1550-1561.

MacDonald, R.W., Solomon, S., Cranston, R.E., Welch, H.E., Yunker, M.B., Gobiel, C.. (1998). A sediment and organic carbon budget for the Canadian Beaufort Shelf. Mar Geol, 144, 255–273.

Manson, G.K., Solomon, S.M., Forbes, D.L., Atkinson, D.E., Craymer, M.. (2005). Spatial variability of factors influencing coastal change in the Western Canadian Arctic. Geo-Mar Lett, 25, 138-145. doi: 10.1007/s00367-004-0195-9.

Manson, G.K., Solomon, S.M. (2007). Past and future forcing of Beaufort Sea coastal change. Atmosphere-Ocean, 45, 107-122.

Mars, J.C., and Houseknecht, D.W.. (2007). Quantitative remote sensing study indicates doubling of coastal erosion rate in past 50 yr along a segment of the Arctic coast of Alaska. Geology, 35(7): 583–586. doi: 10.1130/G23672A.1.

Melling, H., Reidel, D.A., Gedalof, Z., (2005). Trends in the draft and extent of seasonal pack ice, Canadian Beaufort Sea. Geophys. Res. Lett., 32.

Murton, J.B., French, H. M., Lamonthe, M. (1997). 'Late Wisconsinan erosion and eolian deposition, Summer Island area, Pleistocene Mackenzie Delta, Northwest Territories: optical dating and implications for glacial chronology' *Canadian Journal of Earth Sciences*, 34 (2), p190-199, https://doi.org/10.1139/e17-015

Murton, J.B.. (2009). Stratigraphy and paleoenvironments of Richards Island and the eastern Beaufort continental shelf during the last glacial-interglacial cycle. Permafrost and Periglacial Processes, 20, 107-125. doi: 10.1002/ppp.647

Nielsen, D., Pieper, P., Badrkhordarian, A., Overduin, P., Iluina, T., Brovkin, V., Baehr, J., Dobrynin, M., (2021). 'Projected increase of Arctic coastal erosion and its sensitivity to warming in the 21st century', *Nature Climate Change*, doi:10.21203/rs.3.rs-634673/v1

Obu, J., Lantuit, H., Fritz, M., Pollard, W.H., Sachs, T., and Günther, F.. (2016). Relation between planimetric and volumetric measurements of permafrost coast erosion: a case study from Herschel Island, western Canadian Arctic. Polar Research., 35: 30313. doi: 10.3402/polar.v35.30313

O'Brien, M.C., Macdonald, R.W., Melling, H., Iseki, K.. (2006). Particle fluxes and geochemistry on the Canadian Beaufort Shelf: implications for sediment transport and deposition. Cont. Shelf Res. 26, 41–81.

Overeem, I., Anderson, R. S., Wobus, C. W., Clow, G. D., Urban, F. E., Matell, N.. (2011). Sea ice loss enhances wave action at the Arctic coast. Geophysical Research Letter., 38, L17503, doi: 10.1029/2011GL048681

O'Brien, M.C., Macdonald, R.W., Melling, H., Iseki, K.. (2006). Particle fluxes and geochemistry on the Canadian Beaufort Shelf: implications for sediment transport and deposition. Cont. Shelf Res. 26, 41–81.

Overland, J. E., Wood, K. R., Muyin, W. (2011) 'Warm Arctic-cold continents: climate impacts of the newly open Arctic Sea' *Polar research*, 30(1), p.15787-14

O'Rourke, M. J. E. (2017). 'Archaeological site vulnerability modelling: the influence of high impact storm events on models of shoreline erosion in the western Canadian Arctic', *Open Archaeology*, 3 (1), p1-16. Doi:10.1515/opar-2017-0001

Pelletier, B.R., and Medioli, B. E. (2014). 'Environmental atlas of the Beaufort Coastlands', *Geological Survey of Canada*, Open File 7619.

Péwé, T. L., Church, R. E., & Andresen, M. J. (1969). *Origin and paleoclimatic significance of large-scale patterned ground in the Donnelly Dome area, Alaska* (Vol. 103). Geological Society of America.

Péwé, T. L. (1966). Paleoclimatic significance of fossil ice wedges. *Biul. peryglac.*, *15*, 65-73.

Pix4D. (2020). Retrieved October 7th, 2019, from Pix4D: https://www.pix4d.com/

Porter, C., Morin, P., Howat, I., Noh, M., Bates, B., Peterman, K., Keesey, S., Schlenk, M., Gardiner, J., Tomko, K., Willis, M., Kelleher, C., Cloutier, M., Husby, E., Foga, S., Nakamura, H., Platson, M., Wethington, M. Jr., Williamson, C., Bauer, G., Enos, J., Arnold, G., Kramer, W., Becker, P., Doshi, A., D'Souza, C., Cummens, P., Laurier, F., Bojesen, M., Porter, C. (2018). 'ArcticDEM', *Harvard Dataverse*, V1, *https://doi.org/10.7910/DVN/OHHUKH* [Accessed March 23, 2020]

Rachold, V., Griogriev, M.N., Are FE, Solomon S, Reimnitz, E., Kassen, H., Antonow, M.. (2000). Coastal erosion vs. riverine sediment discharge in the Arctic shelf seas. International Journal of Earth Sciences, 89, 450-460.

Rachold, V., Lack, M., Grigoriev, M.N.. (2003). A Geo InformationSystem (GIS) for circum-Arctic coastal dynamics. Proceedings of the 8th International Conference on Permafrost, 21-25, 923–927.

Rachold, V., Eicken, H., Gordeev, V.V., Grigoriev, M.N., Hubberten, H.W., Lisitzin, A.P., Shevchenko, V.P., Schirrmeister, L.. (2004) Modern terrigenous organic carbon input to the Arctic Ocean. The Organic Carbon Cycle in the Arctic Ocean, 1, 35-56.

Rachold, V., Are, F.E., Atkinson, D.E., Cherkashov, G., Solomon, S.M.. (2005). Arctic Coastal Dynamics (ACD): an introduction. Geo-Marine Letters, 25, 63-69. doi: 10.1007/s00367-004-0187-9.

Raczynski, R. J. (2017). *Accuracy analysis of products obtained from UAV-borne photogrammetry influenced by various flight parameters.* Master's Thesis, NTNU.

Rampton, V. N. (1987). 'Surficial Geology, Tuktoyaktuk Coastlands, District of Mackenzie, Northwest Territories', *Geological Survey of Canada*, "A" Series Map 1647A, https://doi.org/10.4095/125160

Rampton, V.N.. (1988). Quaternary geology of the Tuktoyaktuk coastlands, Northwest Territories. Geological Survey of Canada, memoir 423.

Reimnitz, E., Graves, S.M., Barnes, P.W.. (1988). Beaufort Sea coastal erosion, sediment flux, shoreline evolution and the erosional shelf profile. US Geol Surv. Map I-1182-G, p 22. Retrieved from: http://www.awi-potsdam.de/acd

Scharffenberg, K.C., Whalen, D., MacPhee, S.A., Marcoux, M., Iacozza, J., Davoren, G., Loseto, L.L., (2019). 'Oceanographic, ecological, and socio-economic impacts of an unusual summer storm in the Mackenzie Estuary', *Arctic Science*, *6*(2), pp.62-76.

Semiletov, I., Pipko, I., Gustafsson, Ö., Anderson, L.G., Sergienko, V., Pugach, S., et al. (2016). Acidification of East Siberian Arctic Shelf waters through addition of freshwater and terrestrial carbon. Nat. Geosci. 9(5): 361–365. doi: 10.1038/ngeo2695

Smith, M. W., & Vericat, D. (2015). From experimental plots to experimental landscapes: topography, erosion and deposition in sub-humid badlands from structure-from-motion photogrammetry. *Earth Surface Processes and Landforms*, *40*(12), 1656-1671.

Solomon, S.M. (2003). The mineral potential of the proposed Mackenzie Delta marine protected areas', *Geological Survey of Canada*, Open File no. 1820.

Solomon, S.M.. (2005). Spatial and temporal variability of shoreline change in the Beaufort-Mackenzie region, Northwest Territories, Canada. Geo-Mar Lett, 25, 127-137. doi: 10.1007/s00367-004-0194-x

Solomon, S.M., Covill, R.. (1995). Impacts of the September 1993 storm on the Beaufort Sea. Proceedings of the 1995 Canadian Coastal Conference, Vol 2, 779–795.

Solomon, S.M., Forbes, D.L., Kierstead, B.. (1994). Coastal impacts of climate change: Beaufort Sea erosion study. Atmospheric Environment Service, Canadian Climate Centre, 94-2, p 35.

Tanski, G., Wagner, D., Knoblauch, C., Fritz, M., Sachs, T., & Lantuit, H. (2019). 'Rapid CO_2 release from eroding permafrost in seawater', *Geophysical Research Letters*, 46, 11, p244-11,252. https//doi.org/10.1029/2019GL084303

Thieler, E. R., Himmelstoss, E. A., Zichichi, J. L., Ergul, A. (2009). 'Digital Shoreline Analysis System (DSAS) version 4.0-an ArcGIS extension for calculating shoreline change', *U.S. Geological Survey*.

Tonkin, T. N., & Midgley, N. G. (2016). Ground-control networks for image based surface reconstruction: An investigation of optimum survey designs using UAV derived imagery and structure-from-motion photogrammetry. *Remote Sensing*, *8*(9), 786.

Turner, D., Lucieer, A., & De Jong, S. M. (2015). Time series analysis of landslide dynamics using an unmanned aerial vehicle (UAV). *Remote Sensing*, *7*(2), 1736-1757.

van Everdingen, R.. (1998) .Multi-Language Glossary of Permafrost and Related Ground-Ice Terms. National Snow and Ice Data Center/ World Data Center for Glaciology, Boulder, CO.

Walker, H.J., (1988). Permafrost and coastal processes. Proc. 5th Int. Permafrost Conference, vol. 3, 35-42.

Westoby, M. J., Brasington, J., Glasser, N. F., Hambrey, M. J., & Reynolds, J. M. (2012). 'Structure-from-Motion'photogrammetry: A low-cost, effective tool for geoscience applications. *Geomorphology*, *179*, 300-314.

Wheaton, J. M., Brasington, J., Darby, S. E., & Sear, D. A. (2010). Accounting for uncertainty in DEMs from repeat topographic surveys: improved sediment budgets. *Earth surface processes and landforms: the journal of the British Geomorphological Research Group*, *35*(2), 136-156.

Wobus, C., Anderson, R., Overeem, I., Matell, N., Clow, G., Urban, F.. (2011). Thermal erosion of a permafrost coastline: Improving process-based models using time-lapse photography. Arctic, Antarctic, and Alpine Research 43, 474–484.

Williams, P.J., Smith, M.W.. (1989). The Frozen Earth: Fundamentals of Geocryology. Cambridge University Press, Cambridge, UK.

Wolfe, S. A, Dallimore, S.R. and Solomon, S.M.. (1998). Coastal permafrost investigations along a rapidly eroding shoreline, Tuktoyaktuk, N.W.T. In Proceeedings of the 7th International Conference on Permafrost, 55, 1125-1131. Retrieved from: http://research.iarc.uaf.edu/NICOP/DVD/ICOP%201998%20Permafrost%207th%20conf/CD-ROM/Proceedings/PDF001189/170160.pdf

Wolfe, S.A., Kotler, E., Dallimore, S.R.. (2001). Surficial characteristics and the distribution of thaw landforms (1970 to 1999), Shingle Point to Kay Point, Yukon Territory. Geological Survey of Canada, Open File no. 4115.